AD-A147 705 GRAIN REFINING AND MICROSTRUCTURAL MODIFICATION DURING 1/1
SOLIDIFICATION(U) FLORIDA UNIV GAINESVILLE DEPT OF
MATERIALS SCIENCE AND ENGINEERING G J ABBASCHIAN
UNCLASSIFIED OCT 84 N00014-81-K-0730 F/G 11/6 NL

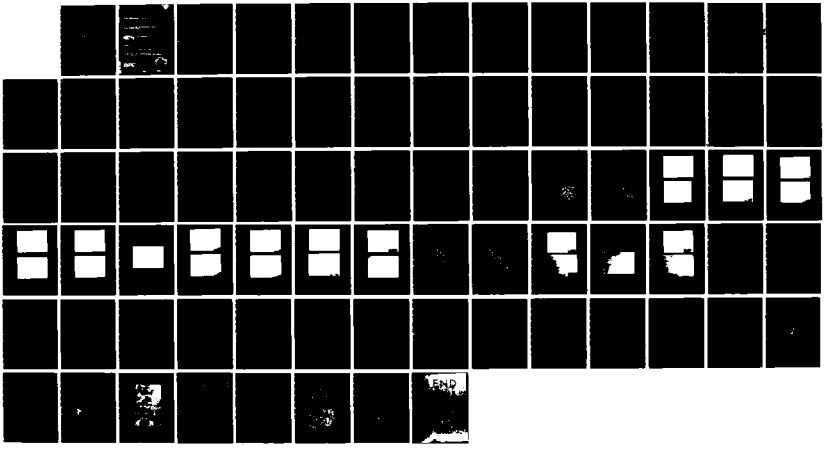

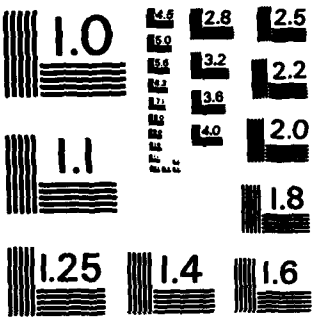

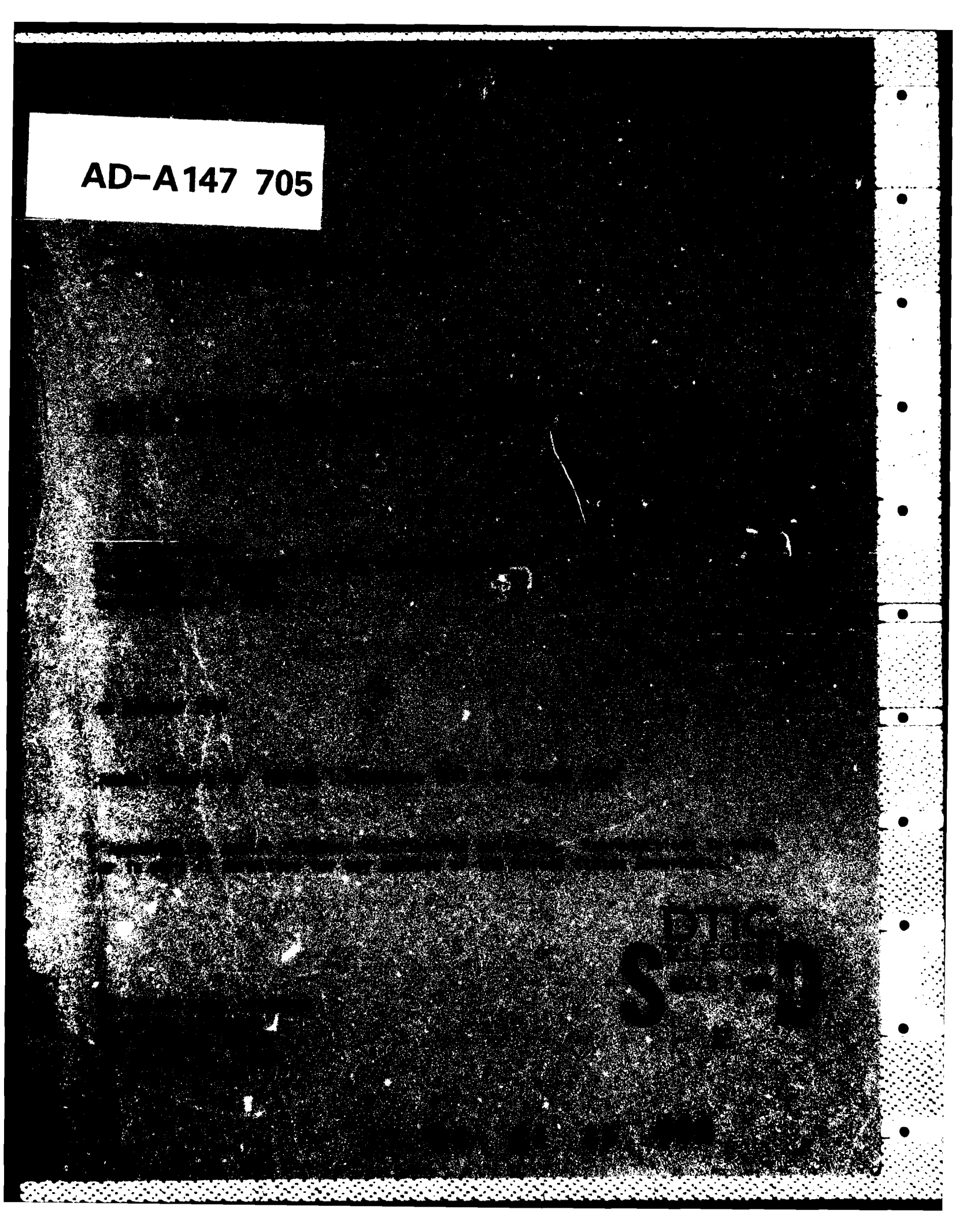

Unclassified

SECURITY CLASSIFICATION OF THIS PAGE (When Date Entered)

REPORT DOCUMENTATION PAGE	READ INSTRUCTIONS BEFORE COMPLETING FORM
1. REPORT NUMBER: 3	2. GOVT ACCESSION NO: AD-A147703
3. RECIPIENT'S CATALOG NUMBER:	
4. TITLE (and Subtitle): GRAIN REFINING AND MICROSTRUCTURAL MODIFICATION DURING SOLIDIFICATION	5. TYPE OF REPORT & PERIOD COVERED: Annual Report September 1983-August 1984
	6. PERFORMING ORG. REPORT NUMBER:
7. AUTHOR(s): G. J. Abbaschian	8. CONTRACT OR GRANT NUMBER(s): N00014-81-K-0730; NR031-836
9. PERFORMING ORGANIZATION NAME AND ADDRESS: University of Florida, Department of Materials Science & Engineering, Gainesville, Florida 32611	10. PROGRAM ELEMENT, PROJECT, TASK AREA & WORK UNIT NUMBERS:
11. CONTROLLING OFFICE NAME AND ADDRESS: Department of the Navy, Materials Division - Office of Naval Research, Arlington, Virginia 22217	12. REPORT DATE: October 1984
	13. NUMBER OF PAGES: 69
14. MONITORING AGENCY NAME & ADDRESS (if different from Controlling Office)	15. SECURITY CLASS. (of this report): Unclassified
	15a. DECLASSIFICATION/DOWNGRADING SCHEDULE:

16. DISTRIBUTION STATEMENT (of this Report)

Approved for public release; distribution unlimited. Reproduction in whole or in part is permitted for any purpose of the United States government.

17. DISTRIBUTION STATEMENT (of the abstract entered in Block 20, if different from Report)

18. SUPPLEMENTARY NOTES

19. KEY WORDS (Continue on reverse side if necessary and identify by block number)

Grain refining, microstructure, solidification, phase diagrams, electromagnetic stirring, Cu-Fe alloys, and Cr-Ni alloys.

20. ABSTRACT (Continue on reverse side if necessary and identify by block number)

This is the third annual report of a research program to study grain refining and microstructural modifications during solidification, as affected by supercooling, solidification rate, and/or inoculation. The report covers results of the current investigations on the structure and phase transformation in Chromium-Nickel alloys (part A), and the final report on the grain refining in copper by the addition of iron and electromagnetic stirring (part B).

DD FORM 1 JAN 73 1473 EDITION OF 1 NOV 65 IS OBSOLETE
S/N 0102-014-6601 |

Unclassified

SECURITY CLASSIFICATION OF THIS PAGE (When Date Entered)

High temperature phase transformations in Cr-Ni binary alloys were evaluated using microstructural, thermal, and TEM analyses of levitation melted binary alloys. The Cr-rich alloys, prepared from 99.9999% and 99.999% pure Cr and Ni, respectively, were levitated in an inert atmosphere containing about 1×10^{-15} ppm oxygen. The results indicate the commonly accepted simple eutectic diagram to be incorrect. Microstructural results show an additional peritectic reaction occurring in alloys containing more than 62 w/o chromium. The peritectic temperature was determined to be in the range of 1420-1475°C, and its composition was in the range of 62 to 70 w/o chromium. Changing the oxygen content of the processing gas from 1×10^{-15} ppm to 6 ppm reduced the peritectic and liquidus temperatures.

The effect of iron additions in the range of 0.57 to 7.5 w/o and electromagnetic stirring on the grain size of electromagnetically levitated copper-iron alloys were investigated. The samples were solidified while levitated or quenched in water from the molten state. The addition of iron was found to be effective in reducing the grain size of copper, and the average grain size decreased as the iron content was increased up to the peritectic liquid composition of about 2.8 w/o Fe. Beyond this composition, the grain size of the samples solidified in the levitated state was insensitive to the iron content, whereas that of the quenched samples continously decreased with increasing iron content. The results also indicate that electromagnetic stirring causes fragmentation of copper dendrites in the hypoperitectic region, and hence enhances grain refinement. In the hyperperitectic region, on the other hand, the stirring has a detrimental effect of the grain refinement by agglomerating the primary iron particles which act as heterogeneous nucleation sites for the copper matrix.

Technical Report No. 3
Contract N00014-81-K-0730; NR031-836

GRAIN REFINING AND MICROSTRUCTURAL MODIFICATION DURING SOLIDIFICATION

G.J. Abbaschian
Department of Materials Science and Engineering
University of Florida
Gainesville, FL 32611

25 October 1984

Annual Report for Period 1 September 1983 - 31 August 1984

OFFICE OF NAVAL RESEARCH
Materials Division
800 N. Quincy Street
Arlington, VA 22217

FOREWORD

This research was supported by the Office of Naval Research, Arlington, Virginia, under contract number N00014-81-K-0730. The scientific officer monitoring the program was Dr. Bruce A. MacDonald. Contributions from Joseph A. Patchett, and Robert Schmees are gratefully acknowledged. Special thanks are due to Professor John Hren, Dr. Stanley Bates, and the staff of the Analytical Instrumental Center for their assistance in the microscopy work, and to Ms. Pam Harrelson for typing the manuscript.

TABLE OF CONTENTS

Abstract

This is the third annual report of a research program to study grain refining and microstructural modifications during solidification, as affected by supercooling, solidification rate, and/or inoculation. The report covers results of the current investigations on the structure and phase transformations in Chromium-Nickel alloys (part A), and the final report on the grain refining in copper by the addition of iron and electromagnetic stirring (part B).

High temperature phase transformations in Cr-Ni binary alloys were evaluated using microstructural, thermal, and TEM analyses of levitation melted binary alloys. The Cr-rich alloys, prepared from 99.9999% and 99.999% pure Cr and Ni, respectively, were levitated in an inert atmosphere containing about 1×10^{-15} ppm oxygen. The results indicate the commonly accepted simple eutectic diagram to be incorrect. Microstructural results show an additional peritectic reaction occurring in alloys containing more than 62 w/o chromium. The peritectic temperature was determined to be in the range of 1420-1475°C, and its composition was in the range of 62 to 70 w/o chromium. Changing the oxygen content of the processing gas from 1×10^{-15} ppm to 6 ppm reduced the peritectic and liquidus temperatures.

The effect of iron additions in the range of 0.57 to 7.5 w/o and electromagnetic stirring on the grain size of electromagnetically levitated copper-iron alloys were investigated. The samples were solidified while levitated or quenched in water from the molten state. The addition of iron was found to be effective in reducing the grain size of copper, and the average grain size decreased as the iron content was increased up to the peritectic

liquid composition of about 2.8 w/o Fe. Beyond this composition, the grain size of the samples solidified in the levitated state was insensitive to the iron content, whereas that of the quenched samples continously decreased with increasing iron content. The results also indicate that electromagnetic stirring causes fragmentation of copper dendrites in the hypoperitectic region, and hence enhances grain refinement. In the hyperperitectic region, on the other hand, the stirring has a detrimental effect on the grain refinement by agglomerating the primary iron particles which act as heterogeneous nucleation sites for the copper matrix.

Part A

Phase Transformations in Binary

Chromium-Nickel Alloys

Introduction

Due to the unique phase stability of the Cr-Ni based alloys at high temperatures, as well as their increased mechanical strength and enhanced corrosion resistance, the importance of understanding the nature of phase transformations in the binary system was recognized as early as the turn of the century. Beginning with the work of Voss (1),Bain (2), and Phebus and Blake (3), it has been indicated that the binary Cr-Ni phase diagram at high temperatures is a simple eutectic system. This proposition has been for the most part accepted with modifications on the phase field limits contributed by several subsequent investigators (4-9). Notwithstanding, there are at present three other proposals on the construction of the Ni-Cr diagram that substantially challenge the proposition of simple eutectic system. Yet these are themselves so radically different from each other, that a great deal of controversy has been generated.

The center of controversy in the Ni-Cr phase diagram lies in determining whether or not chromium undergoes any allotropic transformation that would cause solid-state or eutectoid reactions in the binary alloys. Presently accepted data (10,11) describe the element as b.c.c. below its melting point. Uncertainty as to the value of the melting point has prevailed due to the reactivity of the element, but it has been placed in the range of 1878 ±22°C.

Bloom and Grant (12-14) were the first to report X-ray and

thermal data on a high temperature transformation of chromium, interpreted as being caused by a change from a body centered cubic to a face-centered cubic structure at 1840°C. The high temperature face-centered cubic structure was designated β Cr (15), and was found to result in a eutectoid reaction at 1215°C and a composition of 68 weight percent chromium. However, subsequent experiments (16-20), mostly using sintered powder samples, found no evidence for the Cr allotrope or the eutectoid. Using precipitation techniques, Williams (21) suggested that the rapid and extensive precipitation of the nickel-rich phase may have led Grant and co-workers to misinterpret their data. As a result of these conclusions the proposed diagram was not credited.

Grigor'ev and co-workers (22) in their study of the binary system using X-ray, thermal and microstructural data, have proposed not one, but five polymorphic transformations of chromium resulting in four eutectoid reactions. Their diagram identifies the room temperature chromium as b.c.c., transforming to f.c.c. at 930°C, to b.c.c. at 1300°C, to h.c.p. at 1650°C and then finally to b.c.c. at 1830°C. The eutectoid reactions are placed at 850, 960, 1140, and 1220°C. Additional experiments by the same authors on binary alloys of chromium with tantalum (23), molybdenum (24), iron (25) and tungsten (26) have confirmed the five polymorphic transformations, yet to date no independent study has verified the validity of their conclusions.

A more recent modification of the Cr-Ni diagram has been advanced by Yukawa and co-workers (27). Their diagram has been based on X-ray diffraction data obtained from argon vaporized alloy particles. They have reported an allotrope of chromium, identified as delta phase, which had been reported previously by Kimato and Nishida (28) who used the same technique of vaporizing fine Cr particles in a low pressure argon atmosphere. Yukawa and co-workers, however, extended their work into the Cr-Fe, Cr-Co and the Cr-Ni-Fe systems, and verified the consistent appearance of the delta phase. At compositions ranging from 65 to 70 weight percent chromium, a peritectic reaction involving the nucleation of a sigma phase is also reported at a temperature range from about 1412 to 1270°C. The composition of the sigma phase is reported to be betwen 70 and 75% Cr. The eutectoid reactions are shown to be near 1270 and 1190°C. The existence of the sigma phase in the binary system has in like manner been advanced, based on both experimental data and theoretical considerations, by other researchers. Schuller and Schwaab (29) detected the sigma phase in vacuum deposited Cr-Ni alloy films using an electron microprobe. Their results had been earlier attributed to the presence of impurities (30).

The main difficulty in verifying any of the proposed diagrams is in detecting the high temperature phases. However, this may be due to the limitations of the conventional experimental conditions as well as the very nature of the phases. For instance, sigma phase transformations are character-

istically very sluggish. In ferritic and some austenitic stainless steels, sigma phase forms only where prolonged exposure to high temperatures is experienced, and does not develop by welding or even during heat treating. This may explain why the conventional annealing techniques used to gather X-ray and metallographic data failed to detect the phase. Another problem with most of the aforementioned studies is the contamination of the material by oxygen and other impurities. Kimoto and Nishida (28) have found that the delta phase did not form when oxygen was present in the vaporization chamber.

It may be concluded that though the Ni-Cr system has received a great deal of attention, it remains highly controversial. Part of the controversy may be due to the effect of the experimental techniques, impurities and containers on the solidification of the alloy. To this end, the containerless melting and solidification of high purity bulk samples in an inert atmospheres, as used in the present experiments may lend more accurate information.

Our preliminary research on the solidification of high purity Cr-Ni alloys levitated in an inert atmosphere, reported in the second annual report (31), showed that the commonly accepted Cr-Ni diagram consisting of a simple eutectic at high temperatures is incorrect. Microstructural and thermal arrests results indicated that the diagram should include a eutectic, a peritectic, and a eutectoid for the decomposition of the peritectic phase. The possible existence of a second eutectoid, involving a

high temperature allotropic phase transformation, was also indicated. The solid state transformations were shown to result in the formation of Widmanstätten, basket-weave, blocky, and/or lamellar type morphologies.

This report contains the additional results that have been obtained since the last report. During this period, the experiments have been concentrated in the solid + liquid range of the diagram in order to determine the peritectic temperature and composition more accurately, and also to examine the effect of minute amounts of oxygen impurities on the microstructure.

Samples, prepared from high purity nickel (99.999%) and chromium (99.9999%), were levitated either in a purified inert atmosphere with an oxygen content around 1×10^{-15} ppm or in the as-received inert gas containing about 6 ppm oxygen.

The liquidus temperature and other thermal arrest points of the levitated samples were determined. The experimental procedures were similar to those discussed previously (31,32). The as-quenched samples were evaluated using metallographic, x-ray, and TEM analyses.

RESULTS

Before the experimental results are presented, it would be pertinent to compare the expected microstructures and cooling curves based on the accepted eutectic phase diagram with those of the phase diagram proposed by Yukawa et al.(27) during normal

(non-equilibrium) solidification. For the eutectic diagram, the expected microstructures of Cr-rich alloys would consist of primary α dendrites which initially solidify from the melt. As solidification progresses, the liquid becomes enriched in nickel until the eutectic composition is reached, which then solidifies to form $\alpha + \gamma$. Solid state precipitation of nickel in the α dendrites might take place as temperature is decreased below a certain value. The microstructures is schematically represented in Figure 1, together with the expected cooling curve. A thermal arrest point would occur at the liquidus and at the eutectic temperature of 1345°C where $L \rightleftarrows \alpha + \gamma$. A change of slope or thermal arrest might exist when solid state precipitation takes place.

The microstructure of Cr-rich alloys based on Yukawa's phase diagram, as schematically shown in Figure 2, will have two different features depending on the composition of the alloy; one with primary nucleation of δ, and the other with primary nucleation of σ. If the liquid contains more chromium than the peritectic liquid, pro-peritectic δ dendrites would form first. As solidification progresses, the liquid becomes enriched in nickel and the growing δ dendrites would also become enriched in nickel. Upon further cooling, the σ phase would form via the peritectic reaction, $L + \delta \rightleftarrows \sigma$. The σ phase is expected to form at the liquid-solid interface, covering the surface of the δ dendrite such that the peritectic reaction would not go to completion because of the low solid state diffusion of nickel in

chromium. The liquid will finally solidify eutectically to form $\sigma + \gamma$. As the δ dendrites cool, the chromium-rich core would reach the precipitation temperature of $\delta \rightleftarrows \delta + \alpha$ and the formation of α would be expected at the dendrite cores. Upon further cooling the σ phase would decompose eutectoidally to form $\delta + \gamma$, and δ would finally decompose eutectoidally to form $\alpha + \gamma$. The microstructure is schematically represented by Figure 2.

The expected cooling curve for the above alloy is also shown in Figure 2. A thermal arrest point would occur at the liquidus, at the peritectic temperature and at the eutectic temperature. A change of slope or recalesence may show at the precipitation of α from δ. Another thermal arrest point may occur at the eutectoid decomposition of σ, and at the eutectoid decomposition of δ.

If the liquid contains chromium less than the peritectic liquid, but more than the eutectic, σ dendrites would form first. As solidification progresses, the remaining liquid becomes richer in nickel and finally solidifies eutectically to form $\sigma + \gamma$. As the sample cools, σ will transform similar to the previous alloys. The microstructure is schematically represented in Figure 3, together with the expected cooling curve for this type alloy. A thermal arrest point would occur at the liquidus, at the eutectic temperature, at the eutectoid deomposition of σ, and at the eutectoid deomposition of δ.

It should be noted that the above mentioned transformations can be suppressed by rapid cooling. Also, the indicated thermal arrest points might not be detected if the heat of transformation

is small, or if the transformation takes place over a range of compositions or temperatures. However, the above mentioned features can be used to determine whether or not the eutectic diagram is correct.

In the following sections, microstructural analyses and thermal data are presented for alloys containing 55 to 90 w/o Cr. The experiments, as indicated earlier, were concentrated in the solid and liquid region of the diagram. Two sets of experiments were conducted; in the first set the samples were levitated in the purified inert gas containing 1×10^{-15} ppm oxygen, while in the second set they were levitated in the as-received inert gas containing 6 ppm oxygen.

Microstructures

Microstructures of samples containing 55 to 90 w/o Cr, which were processed in the purified inert gas, are shown in Figures 4 to 11. Some of the samples were etched in a heated and agitated solution of 20 grams potassium ferricyanide, 20 grams potassium hydroxide, and 100 ml of distilled water (called etchant A) for 5 to 15 seconds. The others were etched with aqua regia (called etchant B) for 10 to 25 seconds.

Figure 4 shows the structure of a 55 w/o Cr sample which was quenched in water from its liquidus at 1380°C. The primary Cr dendrites are etched grey, and the interdendritic nickel is etched white. When viewed under polarized light, Figure 4b, Widmansttäten plates are observed inside the primary dendrites.

The structure of another sample with the same composition which was cooled to 1206°C, and held at this temperature for 6 minutes before quenching is shown in Figure 5. At the higher magnification, Figure 5b, nickel lamella, etched white, are observed inside the primary dendrites.

The microstructure of a 62 w/o chromium alloy levitated in the purified gas and quenched at 1413°C is shown in Figure 6. The microstructure when etched with etchant A, Figure 6a, reveals coring within the chromium dendrites, with no apparent boundary between the darker central region and the surrounding parts. However, when the same sample is etched with etchant B, Figure 3b, a clear boundary is observed between the two regions. This structure is similar to microstructures commonly observed during non-equilibrium solidification of alloys involving peritectic-eutectic reactions, as will be shown more clearly later, where the central region represents the pro-peritectic phase and the surrounding part corresponds to the peritectc phase.

The microstructure of a 65 w/o chromium alloys quenched at 1453°C is shown in Figure 7. The microstructure is similar to that of 62 w/o Cr discussed previously, but with larger proportion of the pro-peritectic phase. The pro-peritectic region, is surrounded by a peritectic phase which has undergone solid state decompositon. Figure 8 shows the microstructure of a 71 w/o Cr quenched at 1490°C. Pro-peritectic dendrites are etched white and are surrounded by the darker peritectic phase. The interdendritic region is etched grey. The microstructure is

also shown at a higher magnification in Figure 9, where microhardness indentations are also visible. Various phases of the same region, particularly the decompositon of the peritectic phase, is emphasized using DIC in Figure 9b.

Figure 10 shows the microstructure of a 71 w/o chromium alloy which was melted, cooled to 1372°C, isothermally held at this temperature for 6 minutes and then quenched. At higher magnification, as shown in Figure 10b, a clearly defined peritectic phase, etched white, can be seen. The photomicrographs do not show any precipitation in the peritectic phase. However, TEM analysis, as discussed later, shows that the phase contains fine nickel precipitates.

The microstructure of 78 w/o chromium alloy quenched at 1522°C is shown in Figure 11. The microstructure is similar to those of Figures 6-10, except the amount of pro-peritectic phase is increased, and the interdendritic nickel is decreased considerably. Figure 11 represents the structure of a 90 w/o chromium alloy quenched at 1579°C. The interdendritic nickel can no longer be seen. At higher magnification, Figure 11b, small amounts of peritectic phase surrounding the primary Cr phase can be observed.

The microstructures of the alloys when levitated in the as-received inert gas (containing about 6 ppm oxygen) were similar to those presented earlier, except that the peritectic transformation was not observed in alloys which contained 62 w/o Cr. The Widmansttäten plates and other precipitates also seemed to be much coarser.

Thermal Analysis

The thermal arrest points obtained during normal (non-equilibrium) cooling of the levitated chromium-nickel alloys are given in tables 1 and 2. The first table shows the thermal arrest points of samples which were levitated in the purified gas, and the second table shows the thermal arrest points of samples levitated in the as-received inert gas. The data have been superimposed on the proposed diagram by Yukawa (2) in Figures 12 and 13. The highest thermal arrest points correspond to the liquidus temperatures. It is also the temperature at which the first solid was visually observed to form on the surface of the levitated sample. The transition from the liquid to solid usually occurred rapidly by the formation of a solid shell on the surface. In a few cases, however, solid patches were observed on the surface, which gradually covered the surface as the temperature was reduced.

The other thermal arrest points represent some form of phase transformation or precipitation during non-equilibrium solidification and cooling of the samples, as discussed in more detail later.

X-ray Analysis

Table 8 represents the 2θ values obtained from alloys processed in the purified inert gas, and table 9 represents the values obtained from alloys processed in the as-received inert gas. The diffraction peaks were obtained from a copper target at

room temperature. The calculated lattice parameters are also included in the tables. For comparison, 2θ values and lattice parameters for pure chromium, pure nickel, supersaturated nickel containing 42.19 a/o Cr, and supersaturated chromium containing 38 a/o Ni have also been included. The parameters were obtained from Swanson (33), Pearson (34), Baer (35), and Vagard's law, respectively. The supersaturated compositions correspond to the terminal solid solubility limits at the eutectic temperature. The validity of using Vagard's law to calculate lattice parameters of supercaturated Cr was checked by comparing the calculated lattice parameter of 2.875 Å at 10.7 a/o Ni with a value of 2.877 Å given by Bechtoldt and Vacher (18) for the same alloy.

The X-ray results indicate that, at room temperature, α-Cr and γ-Ni are the only phases present in all but one sample; a 71 w/o chromium processed in the purified inert gas and quenched at 1490°C. This sample showed two extra diffraction peaks at 77.4 and 86.6 degrees. No correlation of these extra peaks could be made with 2θ values reported for the proposed chromium allotropes, chromium-oxygen, nickel-oxygen, or chromium-nickel-oxygen systems.

TEM Analysis

Three samples were analysed using a JOEL 200CX electron microscope; two samples contained 71 w/o Cr and the other contained 90 w/o Cr. One of the first two samples was levitated in

the purified gas, while the others were levitated in the as-received gas.

TEM photomicrographs of the pro-peritectic, peritectic, and interdendritic regions are shown in Figures 14-16, respectively, for the 71 w/o Cr sample processed in the purified gas and quenched at 1375°C. Figure 14 shows that the pro-peritectic region contains fine precipitates. Diffraction patterns obtained from this region indicated the matrix to be bcc chromium, with an approximate lattice parameter of 2.96 Å. The overall composition, matrix plus precipitates, in this region obtained by EDS was in the range of 72-77 w/o, with an average of 75.7 w/o Cr. The peritectic phase as shown in Figure 15, on the other hand, contained platelet precipitates. The overall composition range was 62-70 w/o Cr, with an average around 65.2 w/o Cr. The matrix, similar to the pro-peritectic region, had bcc structure with an approximate lattice parameter of 2.97 Å. The interdendritic region, also containing small precipitates as shown in Figure 15, was fcc and had an average overall composition of 52.4 w/o Cr (with a range of 50 to 53 w/o).

TEM analysis of the other sample containing 71 w/o Cr, levitated in the as-received gas, indicated that its structures are similar to those of the previous sample. However, the precipitates were much coarser than those of the previous sample. Its overall compositions and lattice parameters are given in Table 3. The 90 w/o chromium sample showed only two distinct structures, similar to those of the pro-peritectic and peritectic

regions of the other samples. The pro-peritectic and peritectic regions had overall compositions of 94.6, 77.9 w/o Cr, respectively

Discussion

As discussed earlier, the commonly accepted Cr-Ni diagram at high temperatures consists of a simple eutectic at 1345°C and about 51 w/o chromium. Notwithstanding, there are at present three other proposed diagrams that include, in addition to the eutectic, either a eutectoid (12), a peritectic plus two eutectoids (27), or four eutectoid transformations (22). The major difficulties in studying Cr-Ni phase diagram are due to intense volatilization of Cr at high temperatures, the high affinity of chromium with oxygen, solid state precipitations which may obscure phase transformations, and effects due to impurities. For the present experiment, high purity chromium-nickel binary alloys were levitated in an essentailly oxygen free atmosphere. Thus, the effects of impurities, oxygen, and contamination by a container were eliminated. The temperature was recorded up to 1700°C with an accuracy of ± 10°C with a two color optical pyrometer. Furthermore, rapid quenching technique was employed to preserve the solidification features of the alloys.

The microstructural results indicate that a peritectic reaction occurs in Cr-Ni alloys containing more than 62 w/o Cr. There is a clear and distinct boundary between the pro-peritectic phase and the peritectic phase, ruling out simple coring due to

compositional variation. There is also a difference in the decomposition of the pro-peritectic and the peritectic phases. The former contained fine precipitates, whereas the latter contained Widmansttäten platelets. The fact that the Widmansttäten plates stop at the boundary between the pro-peritectic and peritectic phase, as was shown in the former report (3) and by the TEM results, also indicate a difference in the crystal structure of the two.

The peritectic transformation is not due to the formation of a metastable phase, because this would imply the formation of a metastable peritectic phase on the existing pro-peritectic solid phase. Furthermore, the cooling rate during solidification of the samples in the levitated state was rather slow, around 30°c/sec.

The thermal arrest points obtained during non-equilibrium cooling definitely do not correspond to those expected from the commonly accepted eutectic phase diagram. This is evident from the number of thermal arrest points above the eutectic temperature. The eutectic temperature was found to be 1345°C, as indicated by the sample with 55 w/o chromium which showed the temperature strongly. The arrest points corresponding to the eutectic temperature for alloys with chromium content above 71 w/o chromium were not very clear. This is due to the fact that, as the microstructures of these alloys showed, the amount of the interdendritic region was small.

A thermal arrest around 1442 ± 26°C was observed in most samples containing more than 62 w/o chromium, regardless of the composition, indicating that this temperature is monovarient. Furthermore the peritectic transformation was observed in all the samples that showed this arrest. Therefore, it is believed that this temperature corresponds to the peritectic temperature. Yukawa et al.(27) has proposed a peritectic temperature of 1412°C, and in our previous report (4), based on limited results, this temperature was given around 1410°C.

Another thermal arrest point around 1510°C was observed for the 78 w/o Cr and 71 w/o Cr sample. The temperature seems to be monovarient, although more experiments are necessary to verify this. Nevertheless, the arrest point again cannot be justified based on the simple eutectic diagram. Whether the arrest point corresponds to a precipitation reaction or phase transformation is not clear.

The results also indicate that when the samples were melted in the as-received inert gas, the number of thermal arrest points decreased when compared to those alloys that were processed with the purified inert gas. There was also a noticeable decrease in the liquidus temperature. Therefore, small oxygen content of the purifying gas, as low as 6 ppm, can have a drastic effect on the temperatures as well as the structures. This clearly casts doubt on the results of many previous investigations which did not use high purity gases or used containers which may have reacted with chromium.

The X-ray diffraction results, tables 8 and 9, show 2θ values corresponding to saturated chromium and saturated nickel. The notable exception is the 71 w/o chromium alloy quenched at 1490°C and processed with the purified inert gas. Extra peaks were observed at 77.4 and 86.6 degrees, which did not correspond to any values cited in the literature for chromium, nickel, their alloys or oxides. It should also be noted that there is no difference in the 2θ values when the alloys processed with the as-received inert gas indicating that no appreciable oxygen was dissolved in the alloys.

No 2θ values corresponded to the σ phase because the x-ray patterns were obtained at room temperature and the peritectic structure had decomposed. Thus, it could be inferred that the samples were not quenched fast enough to retain the high temperature phase.

The TEM results also indicated three distinct regions in the 71 w/o chromium sample levitated in the purified gas. The pro-peritectic region containing fine precipitates was bcc, with an average overall composition 75.7 w/o Cr. The peritectic region containing platelet precipitates, also had a bcc structure. Its overall composition ranged from 62-70 w/o Cr, with an average composition around 65.2 w/o chromium. The interdendritic region had fcc structure and an average composition of 52.4 w/o Cr.

The other sample with 71 w/o Cr, the levitated in the as-received gas, had similar characteristics, but slightly lower Cr content. Results of the 90 w/o chromium sample showed only two

distinct regions corresponding to the pro-peritectic and peritectic phases. The former had an overall composition of 94.6, compared with 77.9 w/o for the latter.

Summary

Based on microstructural and thermal analyses, it is clear that a simple eutectic diagram cannot adequately describe the chromium-nickel phase transformations at high temperatures. There is a distinct peritectic phase in alloys containing more than 62 w/o chromium. From thermal analyses, the peritectic temperature was estimated to be around 1442°C, with a standard deviation of 26°C. The eutectic temperature was found to be 1345°C. The liquidus temperatures were determined as 1377, 1449, 1515, 1577, 1628, and 1757°C for 55, 62, 65, 71, 78, and 90 w/o chromium samples, respectively. For 71 w/o chromium samples, the average composition of the peritectic region was around 65.2 w/o Cr. The composition of the interdendritic nickel was around 52.4 w/o Cr. The pro-peritectic region had an average composition of 75.7 w/o Cr.The results of X-ray and TEM analyses indicated that the peritectic phase had transformed to bcc chromium and fcc nickel.

Increasing the oxygen content of the processing gas from 1×10^{-15} ppm to 6 ppm decreased the liquidus temperature drastically, and also shifted the peritectic transformation.

19. W.C. Wyder and M. Hoch: Trans. AIME, 227, 1963, p. 588.

20. D.W. Bare, E.D. Gibson, and O.N. Carlson: Trans. AIME, 230, 1964, p. 934.

21. R.O. Williams: Trans. AIME, 221, 1957, p. 1257.

22. A.T.Grigor ev, E.M. Sokolvskaya, N.A. Nedumov, M.V. Maksimova, L.G. Sokolova and Yeh Yu-pu: Russian Journal of Inorg. Chem., 5, 1961, p. 639.

23. A.T. Grigor ev, L.N. Gusev, E.M. Sokoloskaya and M.V. Makisomova: Rus. J. Inorg. Chem., 4, 1959,p. 984.

24. A.T. Grigor ev, E.M. Sokolovskaya, Yu P. Simanov, J.G. Sokolova, V.N. Pavlos and M.V. Maksimova: Vestnik Moskov, 3, 1960.

25. A.T. Grigor ev, E.M. Sokolovskaya, et al.: Rus. J. Inorg. Chem., 5, 1960, p. 1036.

26. A.T. Grigor ev, et al: Vestnik Moskov, 4, 1961.

27. N. Yukawa, M. Hida, T. Imura, M. Kawamura and Y. Mizuno: Metall. Trans., 3, 1972,p. 887.

28. Kimato and Nishida: J. Phys. Soc. Japan, 22, 1967, p. 744.

29. V. Schuller and P. Schwab: Z. Metallkunde, 11, 1960, p. 81.

30. A. Taylor and R.W. Floyd: J. Inst. Metals, 80, 1951-52, p. 577.

31. G. J. Abbaschian, "Grain Refining and Microstructural Modification during Solidification," Second Annual Report, October 15, 1983, ONR Contract No. N00014-81-K-0730, prepared for the Office of Naval Research, Arlington, VA.

32. G.J. Abbaschian, "Grain Refining and Microstructural Modification during Solidification," First Annual Report, October 20, 1982, ONR Contract No. N00014-81-K-0730, prepared for the Office of Naval Research, Arlington, VA.

33. H.E. Swanson, N.R. Gilfrich, and G.M. Ugrinic: NBS Circular 539, 1955, vol. V, p. 20-21.

34. W.B. Pearson: Handbook of Lattice Spacings and Structures of Metals, Pergamon Press, New York, 1967.

35. H.G. Baer: Z Metallkunde, 49, 1958, p. 614-622.

References

1. G. Voss: Ztsh. fur Anorg. Allgem. Chemie, 57, 1908, p. 34.

2. C.H. Bain: Trans. AIME, 68, 1923, p. 625.

3. W.C. Phebus and F.C. Blake: Physical Review, 25, 1925, p. 107.

4. S. Nishigori and Hamasumi: Science Reports, 8, 1929, p. 491.

5. M. Taski: Proceedings World Engineering Congress, 36, 1929, p. 231.

6. F. Weaver and W. Jellinghaus: Mitteilungen Kaiser-Wilhem-Institut fur Eisenforchung, 13, 1931, p. 93.

7. B. Matsunaga: Japan Nickel Review, 1, 1933, p. 347.

8. E.R. Jette, V.H. Norstrom, B. Quenau and F. Foote: Trans. AIME, 111, 1934, p. 361.

9. C.H.M. Jenkins: Journal Iron and Steel Institute, 136, 1937, p. 193.

10. V.G. Rivlin and G.V. Raynor: International Metals Review, 1, 1980, p. 21.

11. R. Hultgren, P. Desai, D.T. Hawkins, M. Gleiser and K. Kelley: Selected Values of Thermodynamic Properties, ASM, 1970.

12. D.S. Bloom and N.J. Grant: Trans. AIME, 191, 1951, p. 1009.

13. D.S. Bloom and N.J. Grant: Trans. AIME, 194, 1952, p. 524.

14. D.S. Bloom, J.W. Putnam and N.J. Grant: Trans. AIME, 194, 1952, p. 626.

15. C. Stein and N.J. Grant: Journal of Metals, 1955, p. 127.

16. R.G. Ross and Hume-Rothery: J. Less-Common Metals, 5, 1963, p. 258.

17. B.M. Vasyutinskii, G.N. Kartmazov and V.A Finkel: Phys. Metals Metallog., 12, 1961, p. 141.

18. C.J. bechtoldt and H.C. Vacher: Trans. AIME, 221, 1961, p. 14.

Table 1 -Thermal arrest points during non-equilibrium cooling of samples levitated in the purified inert gas.

w/o Cr	Liquidus,°C	Additional Arrest Points			
55	1375			1345	
55	1380				
Average	1377.5±2.5				
62	1452		1421	1366	(1335)
62	1447				(1335)
Average	1449.5±2.5				
65	1500		1423	1359	
65	1511		1430	1382	
65	1534		1474	1405	1350
Average	1515±14.2				
71	1552				
71	1570		1460		
71	1585	1513	1438		
Average	1577±18.8				
78	1641		1458		
78	1610	1504	1435		
78	1633	1533			
78	1627	1501	1447	1385	
Average	1628±11.4				
90	1760		1435		
90	1755		1444		
Average	1757±2.5				

( ) - Temperatures in parentheses represent small slope change in the thermal data, rather clear recalescence.

Table 2- Thermal arrest points during non-equilibrium cooling of samples levitated in the as-received inert gas.

w/o Cr	Liquidus,°C	Additional Arrest Points		
55*	1327	1309		
55*	1305			
55*	1270			
55*	1303			
Average	1301±20			
62	1402	1378		
65	1433	1387		
68	1497		1350	
68	1497	1395	(1342)	1330
68	1497		(1315-1345)	
68	1490	1390		
68	1473		(1320-1345)	
Average	1493±10.7			
71	1503	1402		
71	1494	1436		
71	1520			
Average	1506±10.8			
78	1566	(1536)	1498	1466
78	1558	(1521)		
Average	1562±4			
85	1610	(1560)		
85	1618	(1566)		
85	1596	(1543)		
Average	1608±9			
90	1652	(1549)		
90	1648	(1610)		
90	1656	(1631)		
90	1654	(1596)		
90	1658	(1637)		
Average	1654±3.4			

* - The temperature of these samples became quiesent at about 1460°C, possibly due to the formation of a thin oxide layer on the surface.
( ) - Temperatures in parentheses represent small slope change in the thermal data, rather than clear recalescence.

Table 3 - 2θ values for Cu radiation of samples processed with the purified gas.

		Ni	Cr	Ni	Cr	Ni	Cr	Ni	Ni	Cr	a_o(Å) Cr	Ni
Pure element		44.5	44.4	51.9	64.6	76.4	81.9	93	98.5	98.2	2.88	3.52
Saturated		43.8	47.7	51	65.1	75	82.4	91.1	96.4	99.7	2.86	3.58
w/o Cr	Quench temperature (°C) and holding time (min)											
55	1383-6	43.4	44.4	50.3							2.88	3.62
62	1413-0	44	44.9	51.1	65.4	75	82.6				2.85	3.56
62	1209-6.5	43.7	44.9	50.8		74.7	82.5	90.9	95.9	98.9	2.86	3.59
71*	1490-0	44.2	45	51.2	65.3	75.2	82.4	91			2.86	3.57
78	1447-0		44.5				82.1			98.6	2.88	-
90	1458-0		44.5		64.7		81.8				2.88	-
90			45.2		65.5		82.4			98.8	2.85	-

* Extra peaks at 77.4 and 86.6.

Table 4 - 2θ values for Cu radiation of samples processed with the as-received inert gas.

							a_0(Å)					
		Ni	Cr	Ni	Cr	Ni	Cr	Ni	Ni	Cr	Cr	Ni
	Pure element	44.5	44.4	51.9	64.6	76.4	81.9	93	98.5	98.2	2.88	3.52
	Saturated	43.8	47.7	51	65.1	75	82.4	91.1	96.4	99.7	2.86	3.58
w/o Cr	Quenched temperature (°C) and holding time (min)											
55	1272-67	43.4	44.4	50.6		74.4	82	90.4	95.6		2.88	3.60
55	1207-36	43.6	44.8			74.8			96.1		2.86	3.59
62	1300-4.7	44	44.7		65.3		82	90.7			2.87	3.58
71	1380-3.5		44.6	50.4		75.2	82.3			98.8	2.87	3.60
71	1440-3.5	43.8	44.8	51.2	65		82.3			98.6	2.87	3.57
90	1370-2.8		45		65.1		82.1	91		98	2.87	3.58
90	1490-8		45.4								2.83	-

Table 5 - Lattice parameters crystal structures, and overall compositions.

	Region	a_o(Å)	Structure w/o Cr	Overall
71 w/o Cr, Purified gas	Pro-peritectic	2.96*	bcc	75.7
	Peritectic	2.97*	bcc	65.3
	Interdendritic	3.74*	fcc	52.4
71 w/o Cr, As-received gas	Pro-peritectic	-	-	72.3
	Peritectic	2.90*	bcc	60.9
	Interdendritic	3.58*	fcc	51.9
90 w/o Cr, As-received gas	Pro-peritectic	2.97*	bcc	94.6
	Interdendritic	2.95*	bcc	77.9

* The lattice parameters for the matrices are given for comparison purposes only. More accurate values of the parameters are given by the X-ray results in tables 3 and 4.

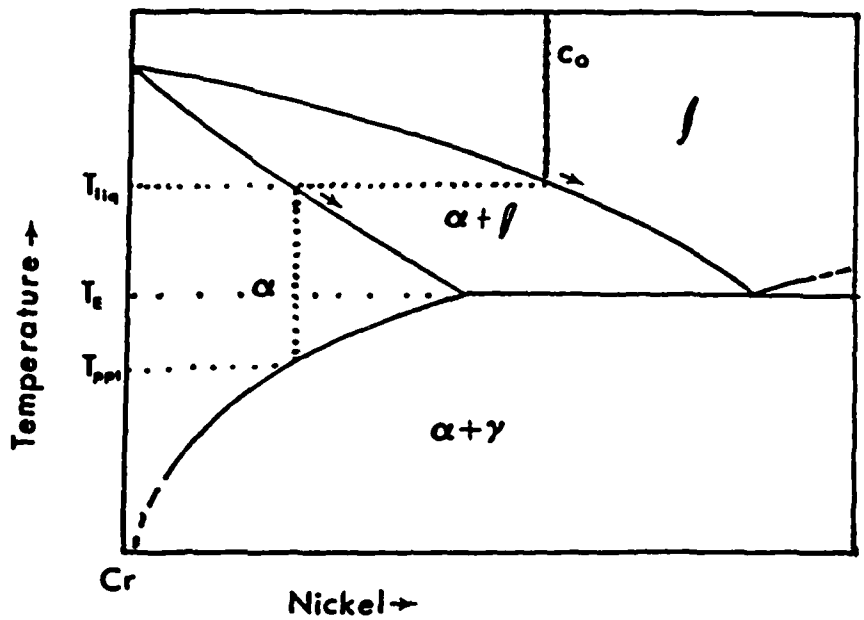

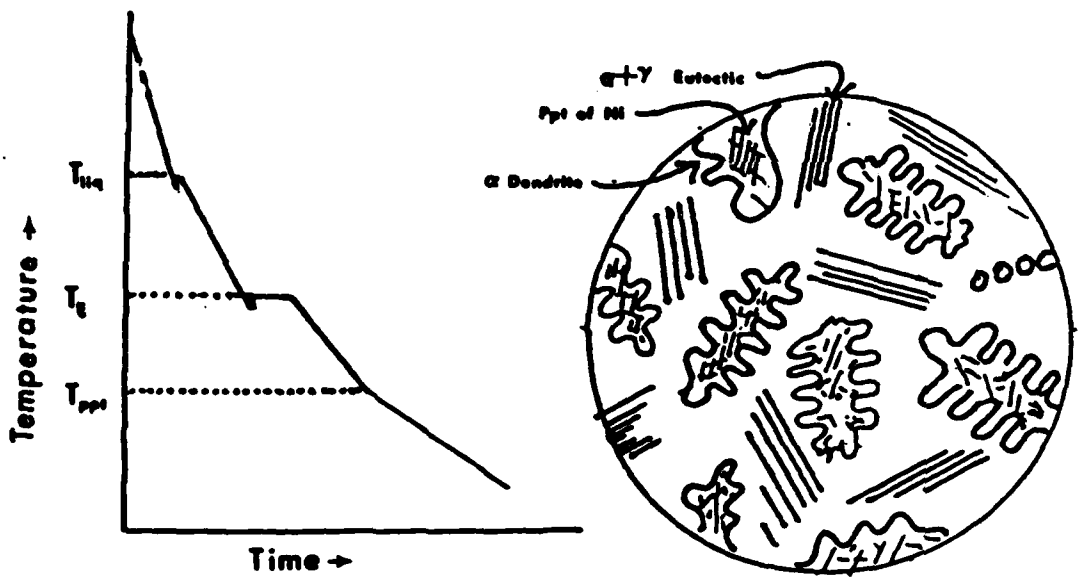

Figure 1 Schematic microstructure and cooling curve for chromium-rich alloys, as expected from the accepted eutectic phase diagram.

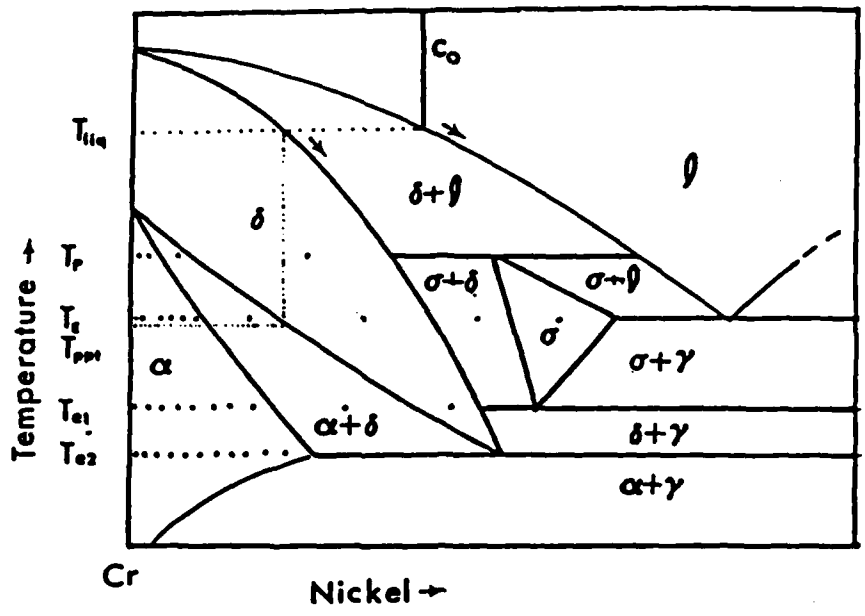

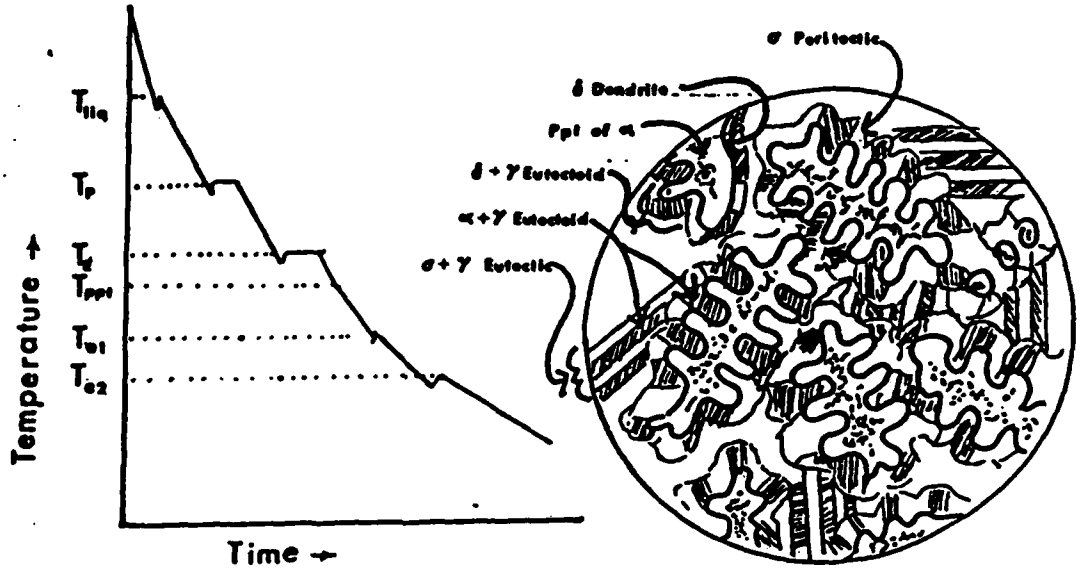

Figure 2 Schematic microstructures and cooling curve for chromium-rich alloys, with primary nucleation of δ from the melt, as expected from the Yukawa's proposed diagram (27).

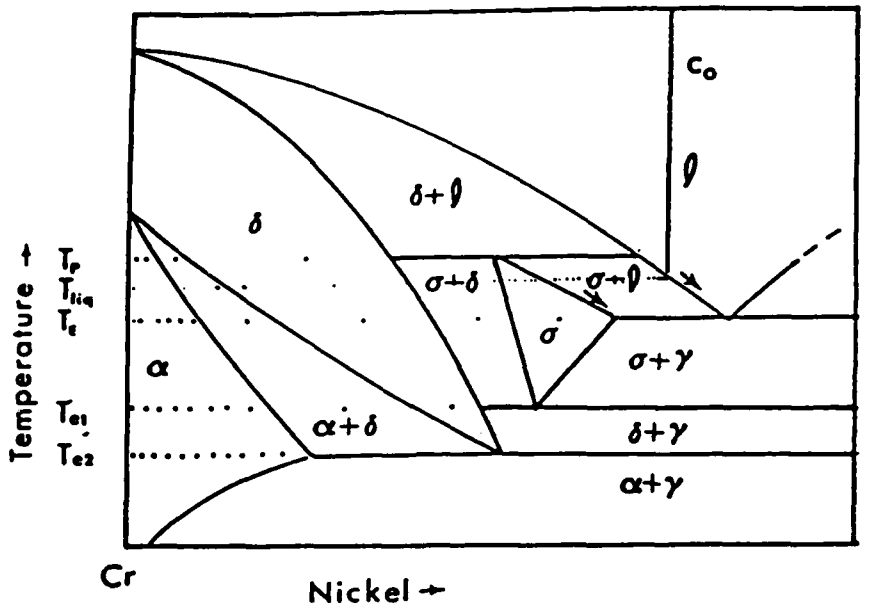

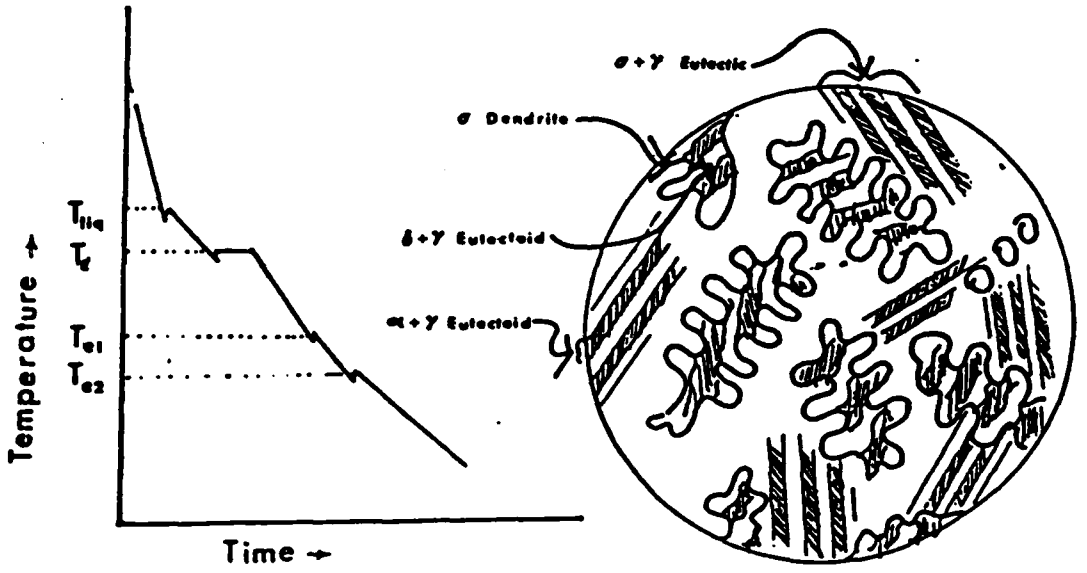

Figure 3 Microstructures and cooling curve for chromium-rich alloys, with primary nucleation of σ from the melt, as expected from Yukawa's proposed diagram (27).

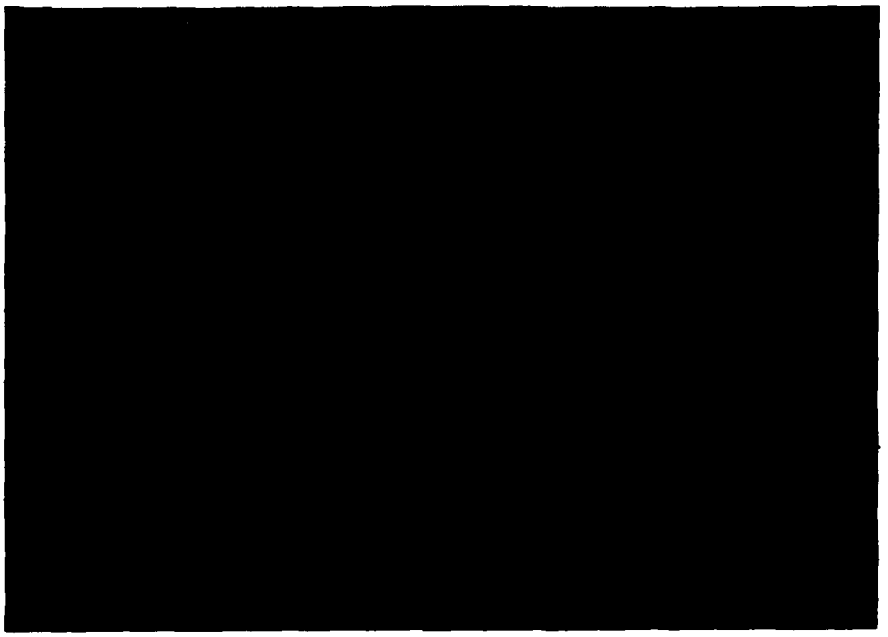

a

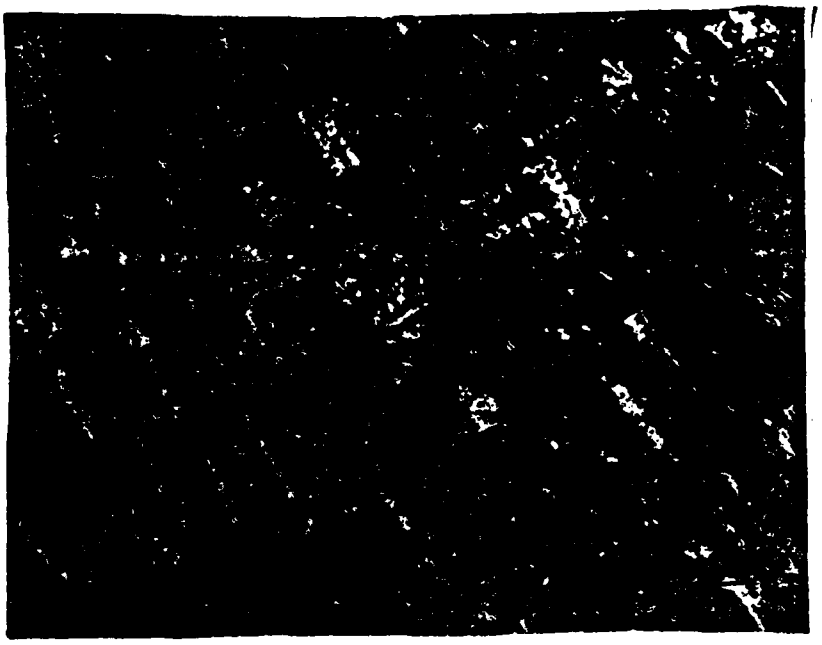

b

Figure 4 Microstructure of 55 w/o chromium alloy quenched at 1380°C: (a) viewed under brightfield, and (b) viewed under polarized light. Etchant B.

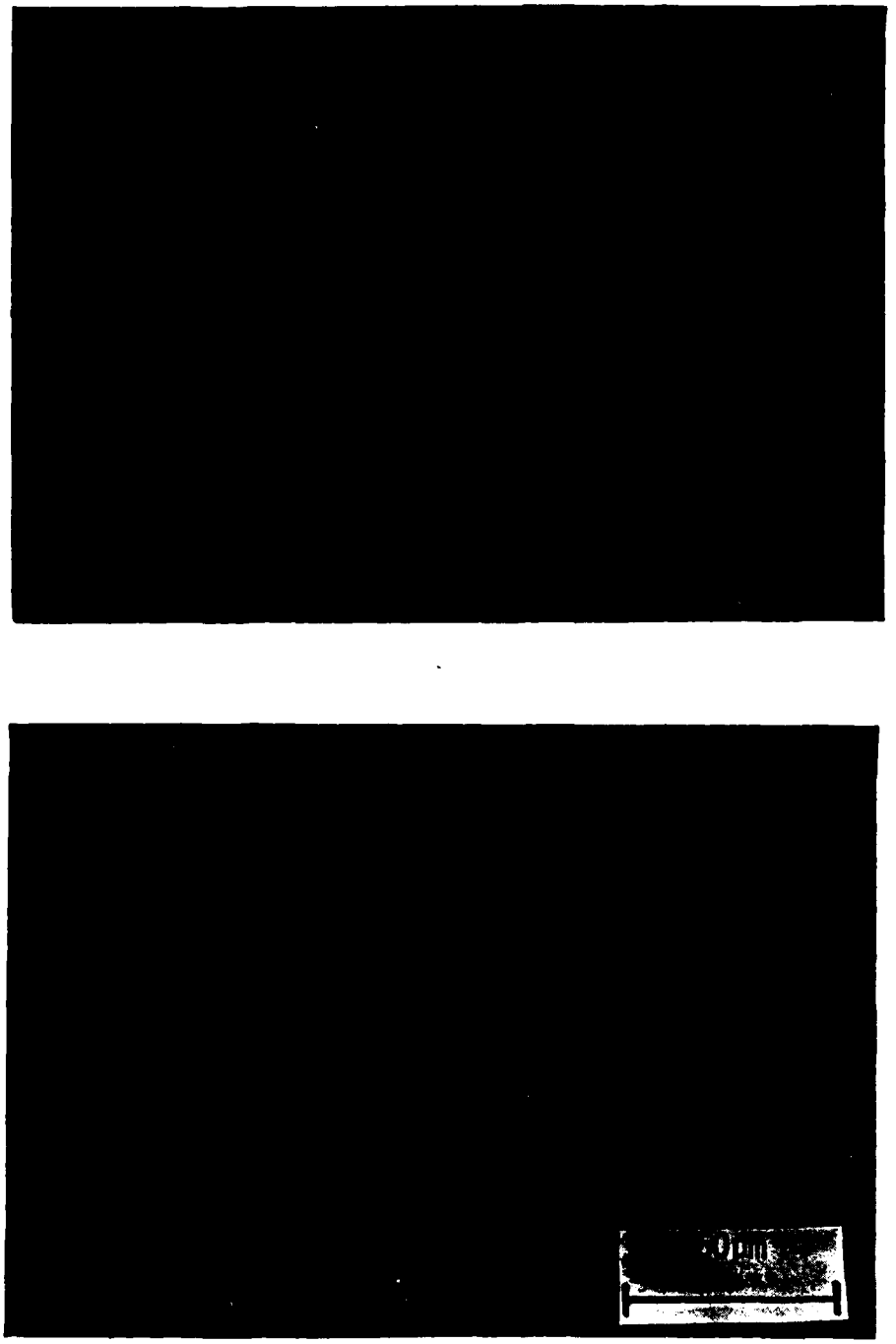

Figure 5 Microstructure of 55 w/o chromium alloy quenched at 1206°C after holding at this temperature for 6 minutes. Etchant B.

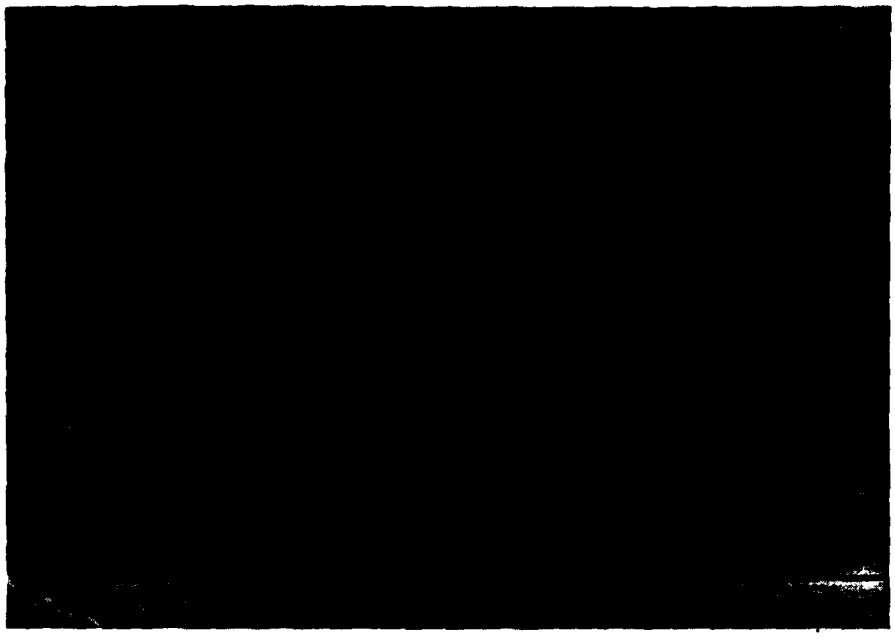

a

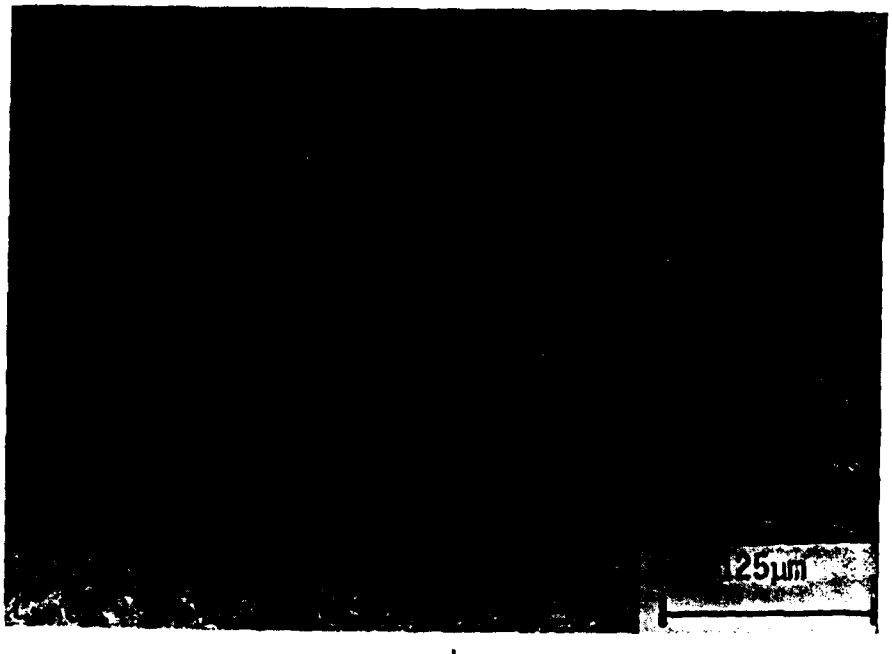

b

Figure 6 Microstructure of 62 w/o chromium alloy quenched at 1413°C: (a) etched with etchant A, and (b) etched with etchant B.

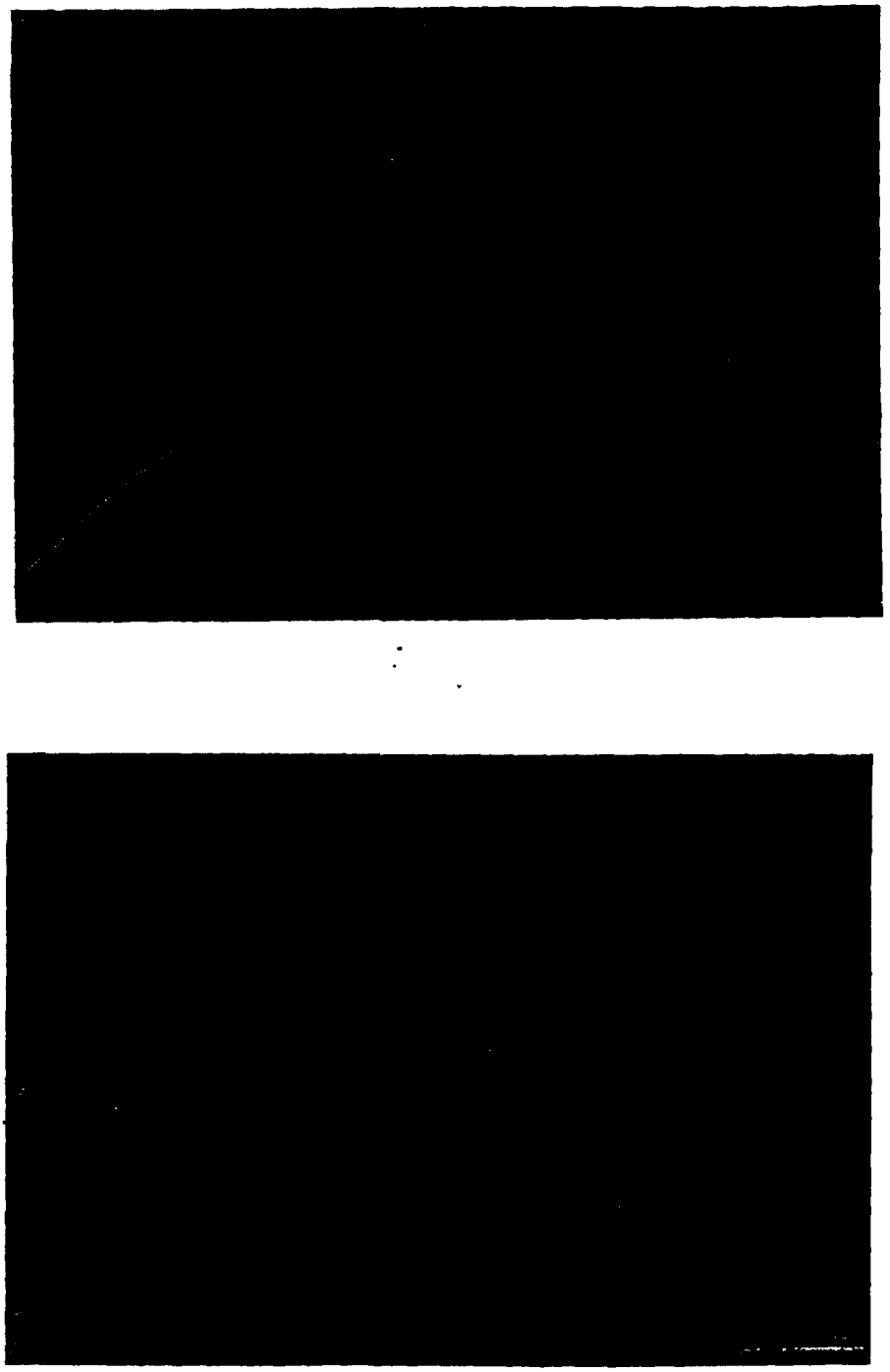

Figure 7 Microstructure of 65 w/o chromium alloy quenched at 1453°C. Etchant B.

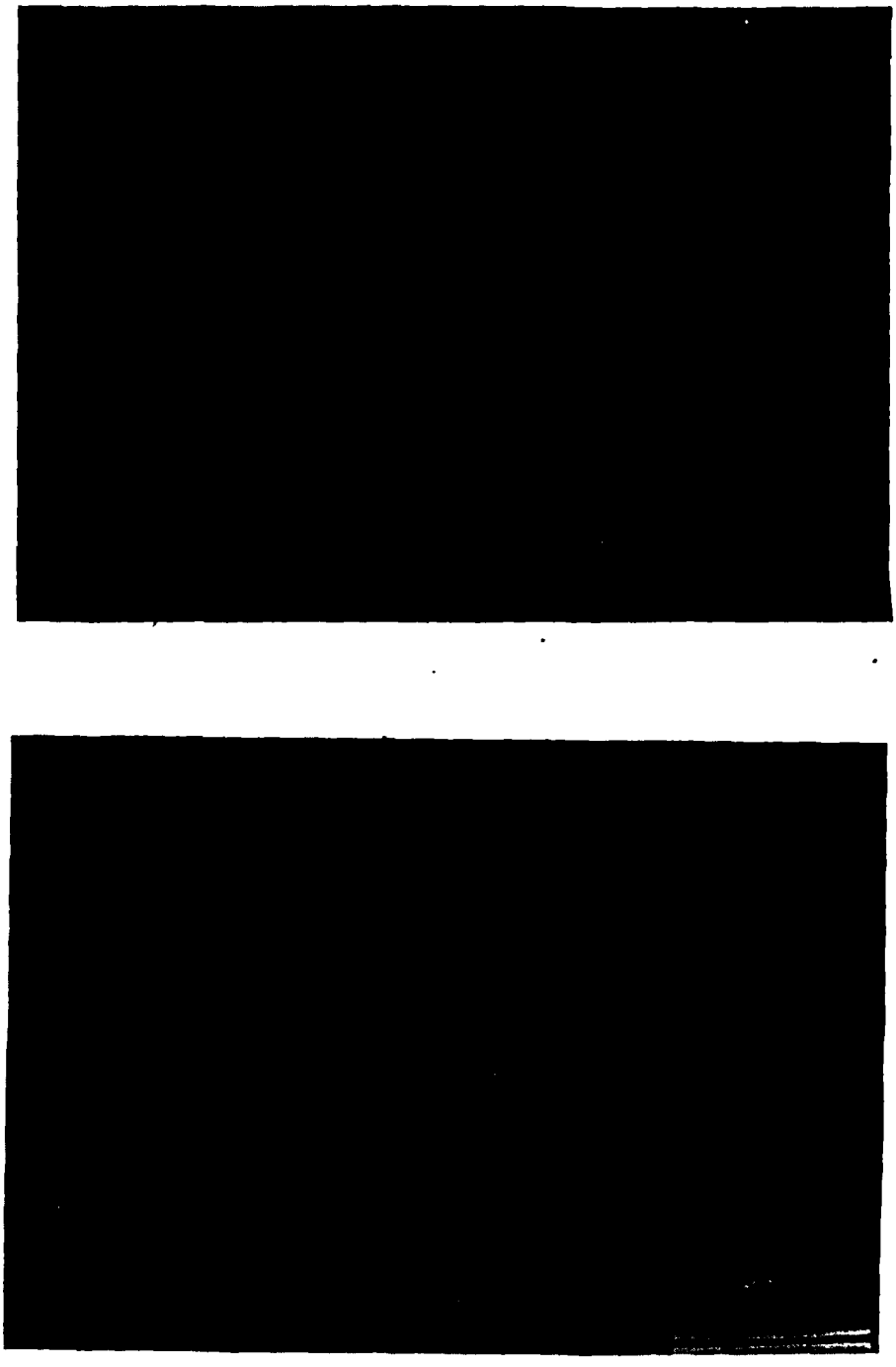

Figure 8 Microstructure of 65 w/o chromium alloy quenched at 1444°C; viewed under DIC. Etchant B.

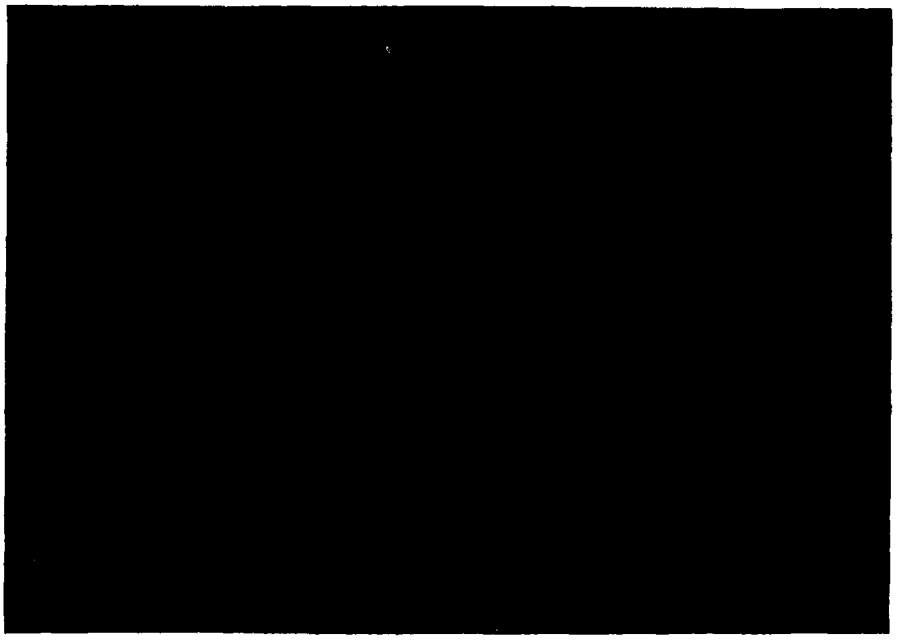

Figure 9 Microstructure of 71 w/o chromium alloy quenched at 1490°C. Etchant A.

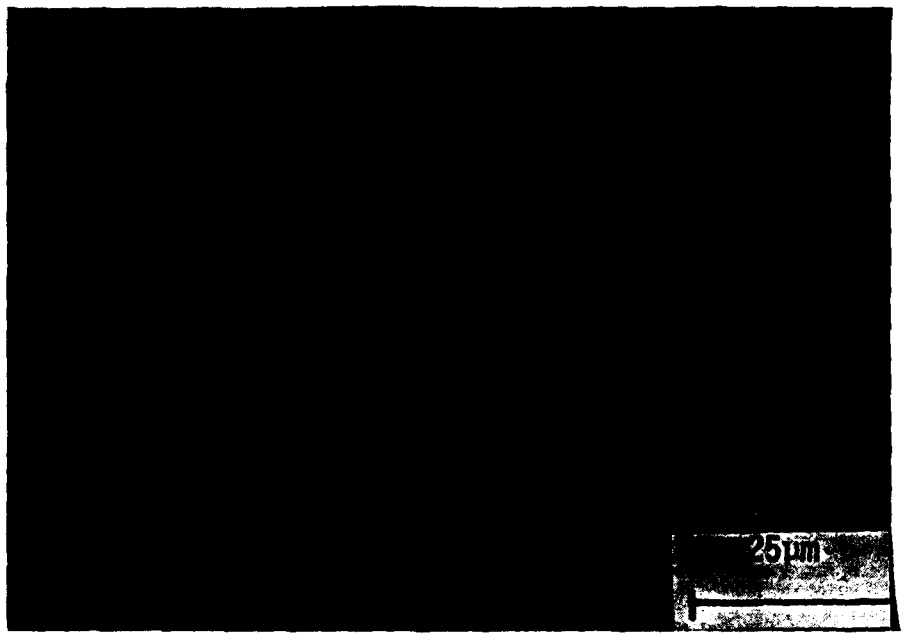

a

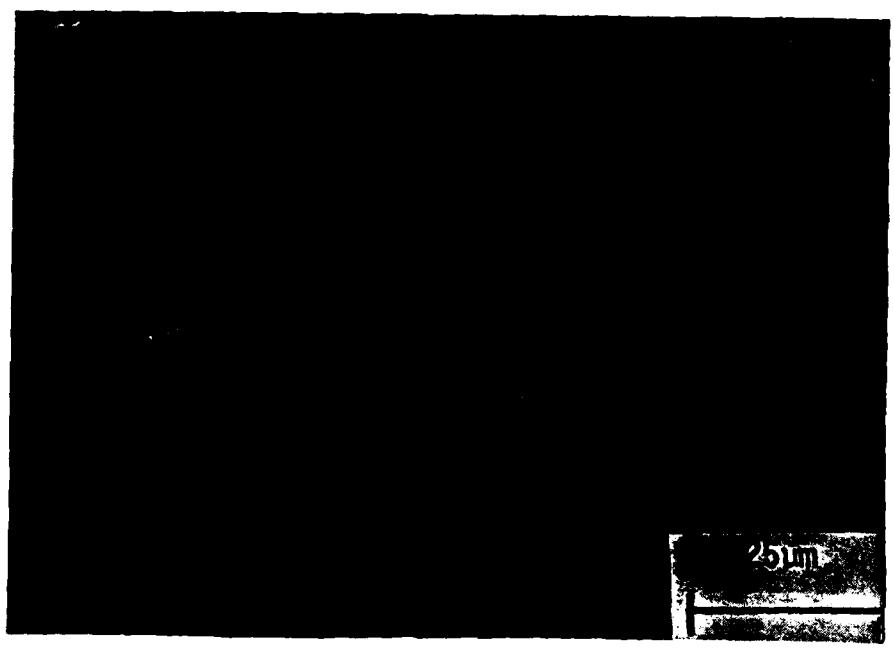

b

Figure 10 Microstructure of 71 w/o chromium alloy quenched at 1490°C: (a) viewed under brightfield, and (b) viewed under DIC. Etchant B.

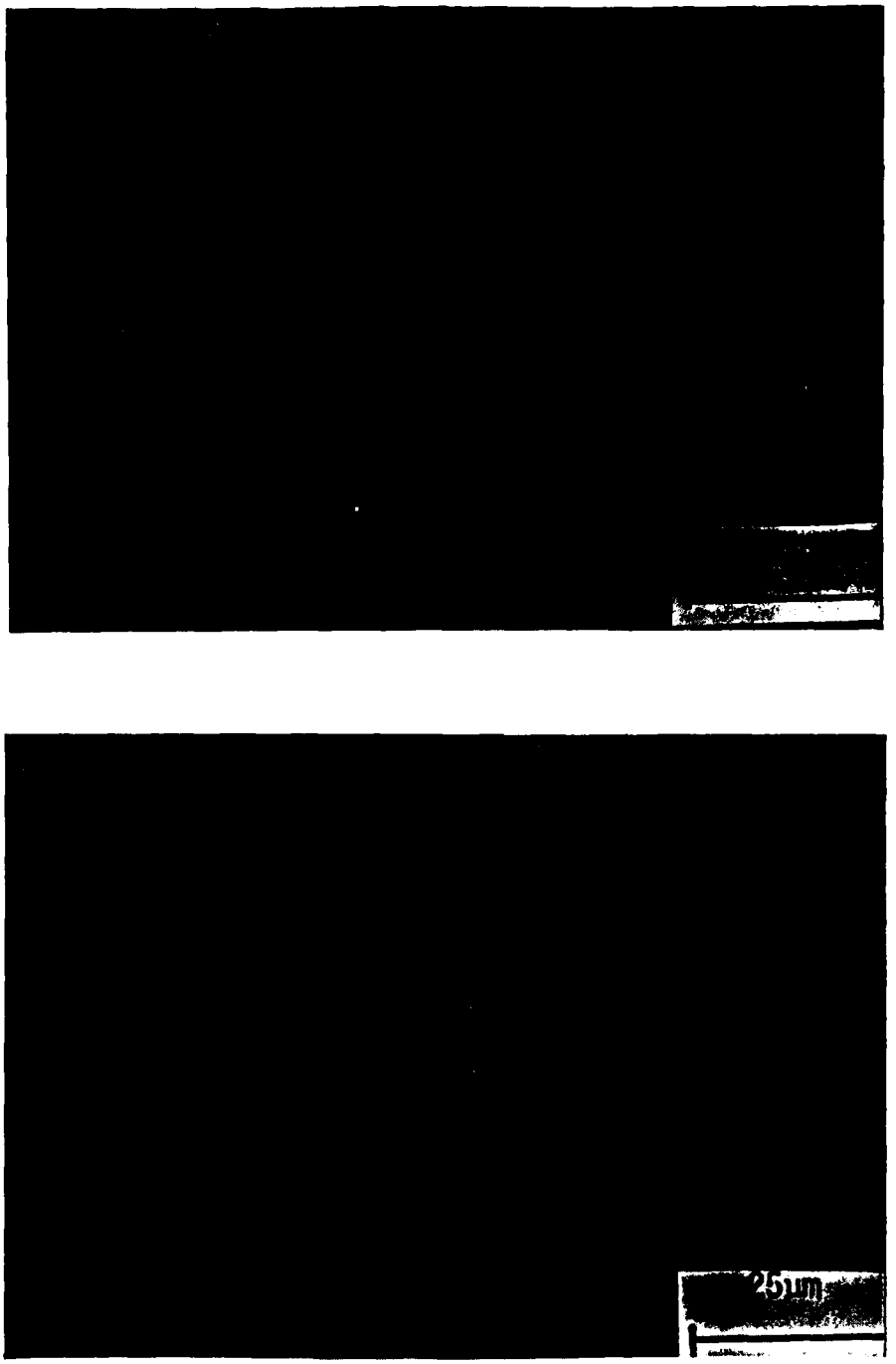

Figure 11 Microstructure of 71 w/o chromium alloy quenched at 1372°C, after holding at this temperature for 6 minutes. Etchant A.

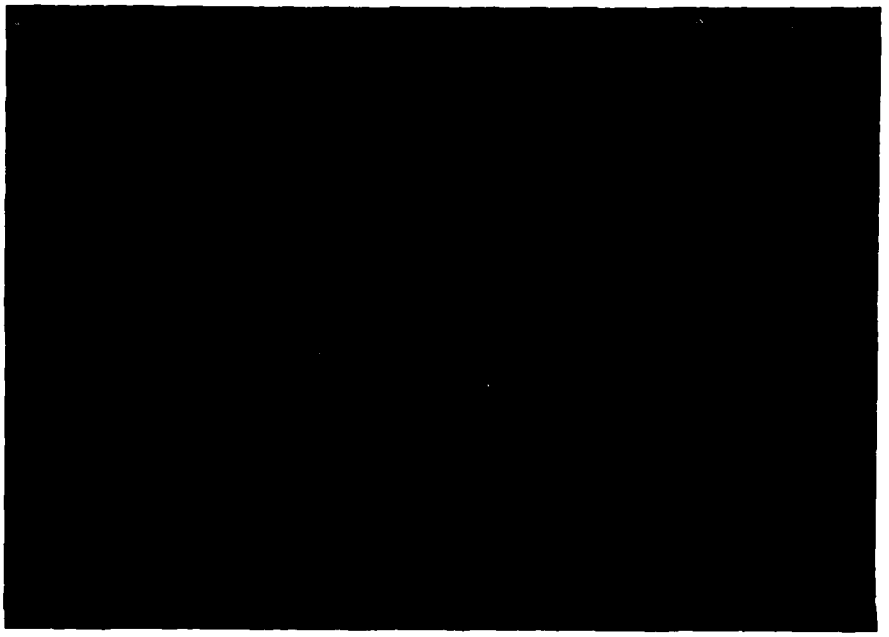

a

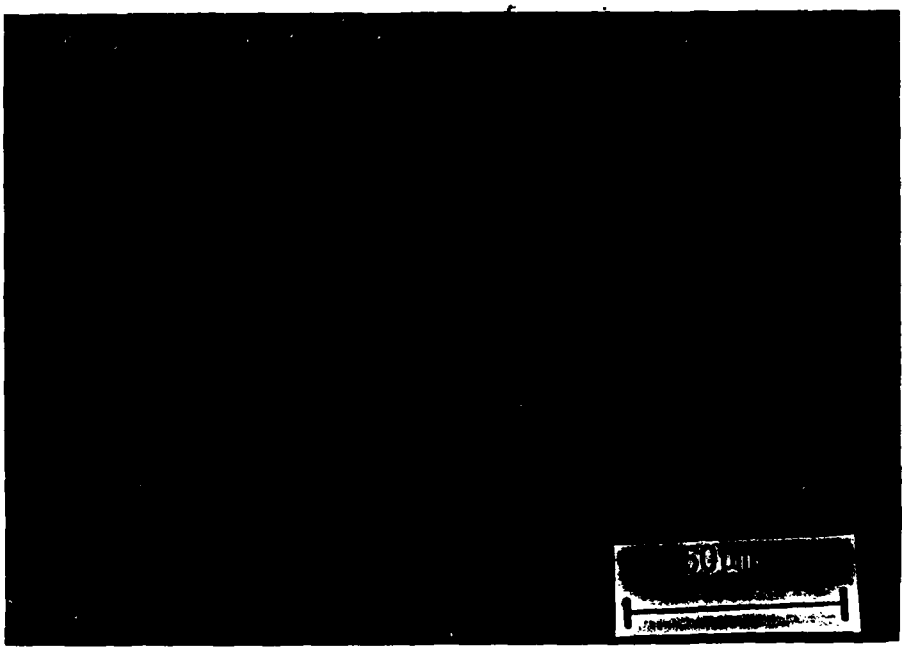

b

Figure 12 Microstructure of 78b w/o chromium alloy quenched at 1400°C: (a) etched with etchant B followed by etchant A and viewed under brightfield; (b) etched with etchant B and viewed under DIC.

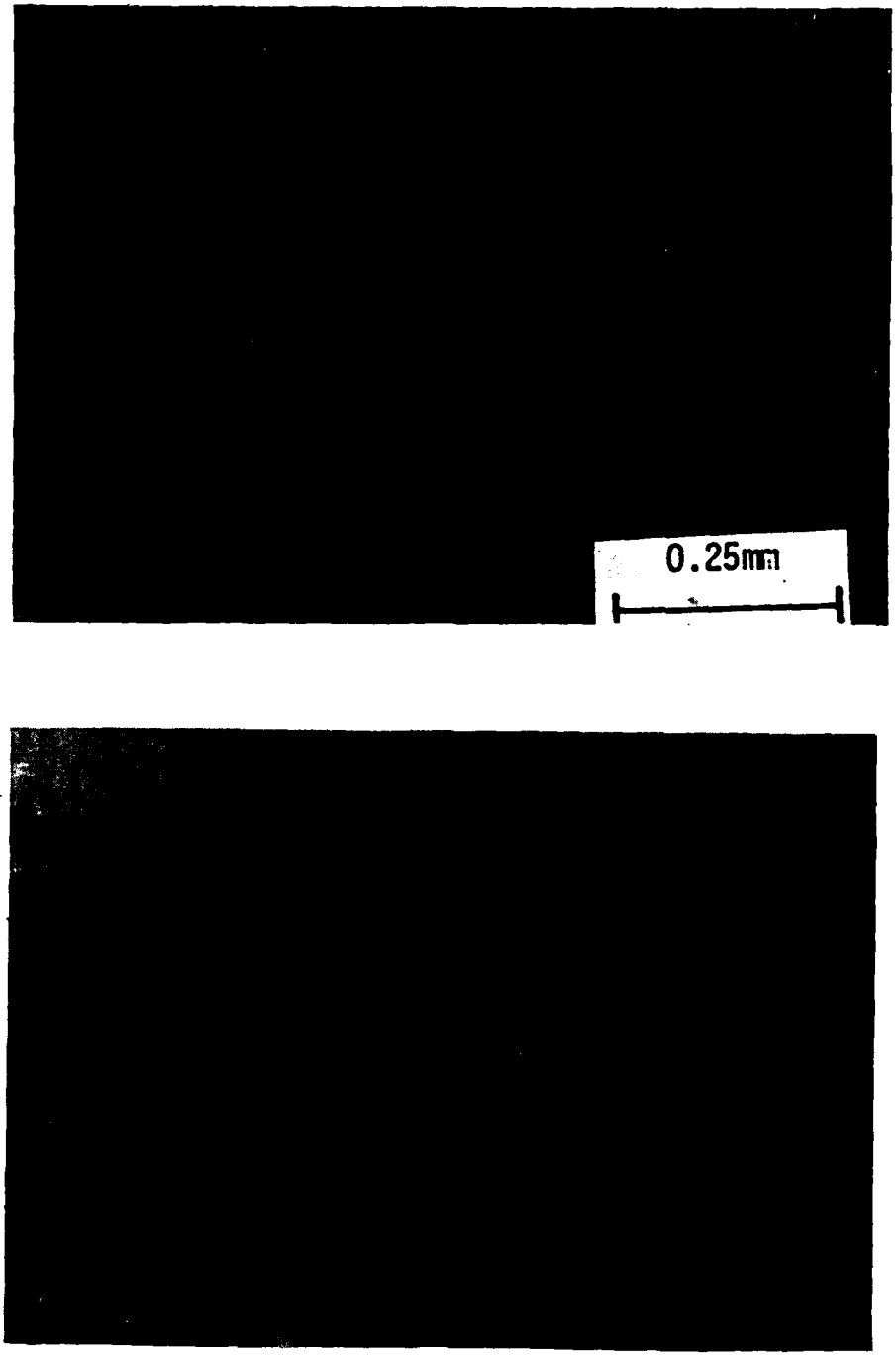

Figure 13 Microstructrure of 90 w/o chromium alloy quenched at 1459°C. Etchant B.

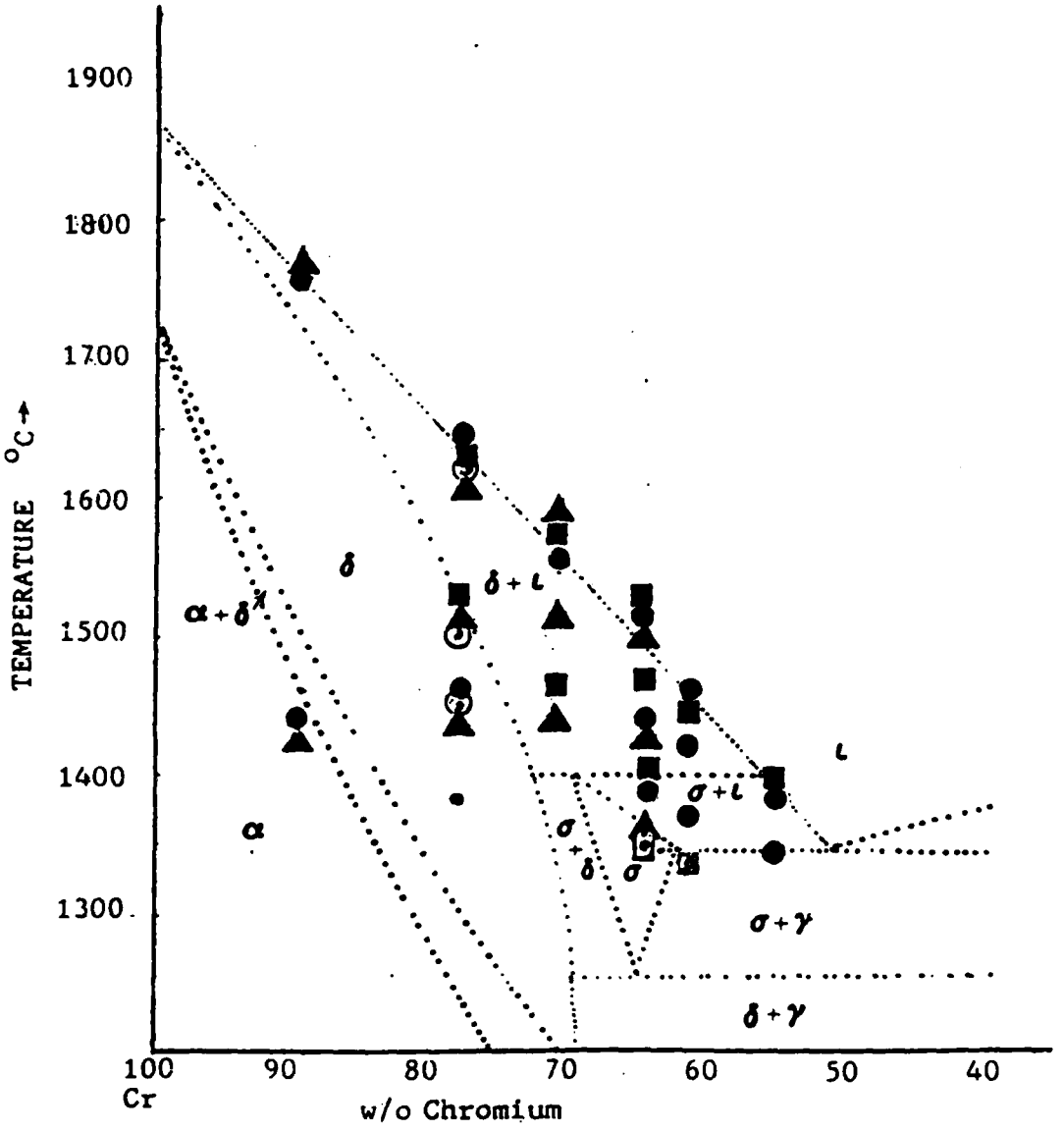

Figure 14 Thermal arrest points of levitated chromium-nickel alloys processed with purified inert gas, superimposed on Yukawa's phase diagram.

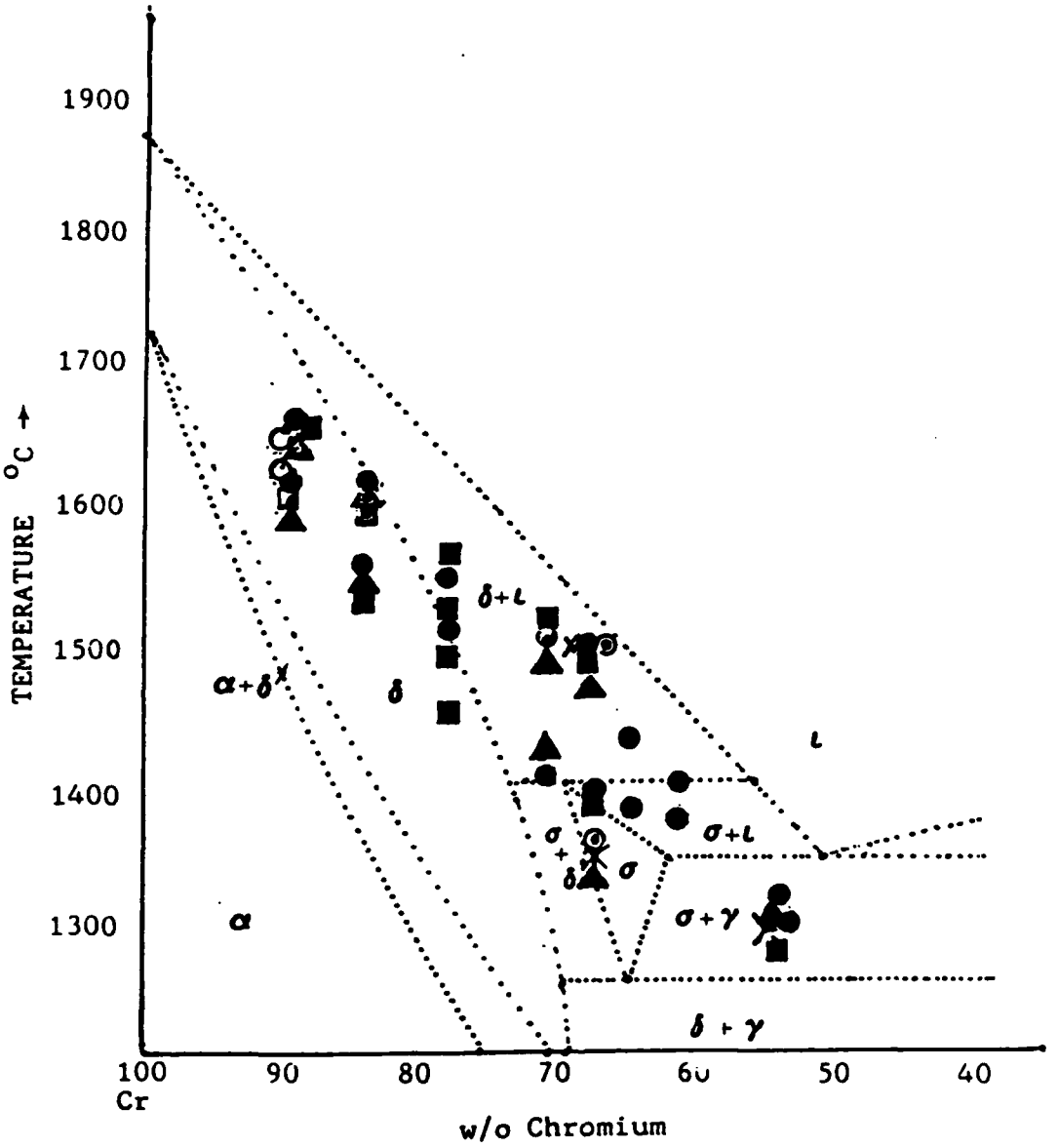

Figure 15 Thermal arrest points of levitated chromium-nickel alloys processed with as-received inert gas superimposed on Yukawa's phase diagram.

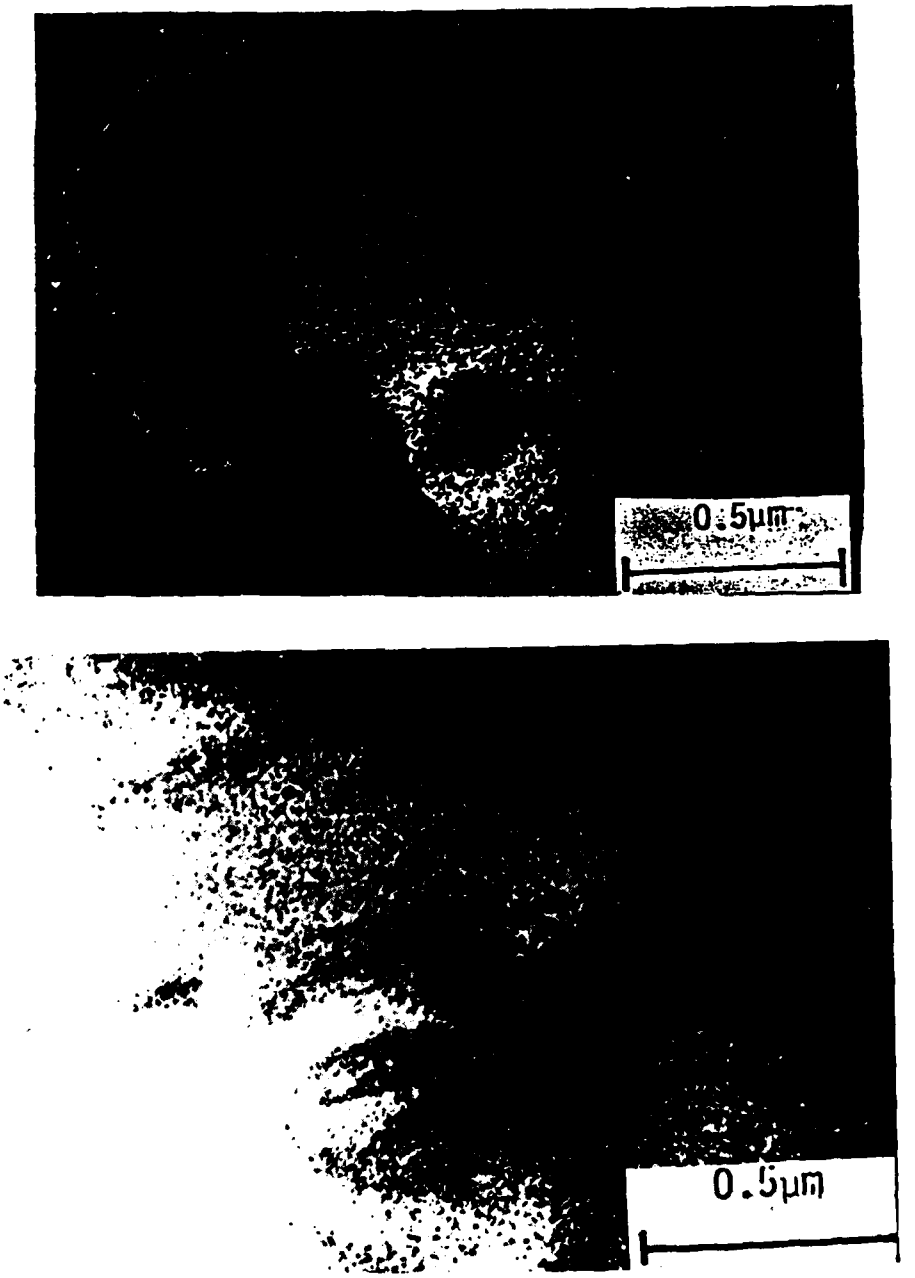

Figure 16 Comparison of darkfield and brightfield TEM photomicrographs from the pro-peritectic region of a 71 w/o chromium sample processed with purified inert gas.

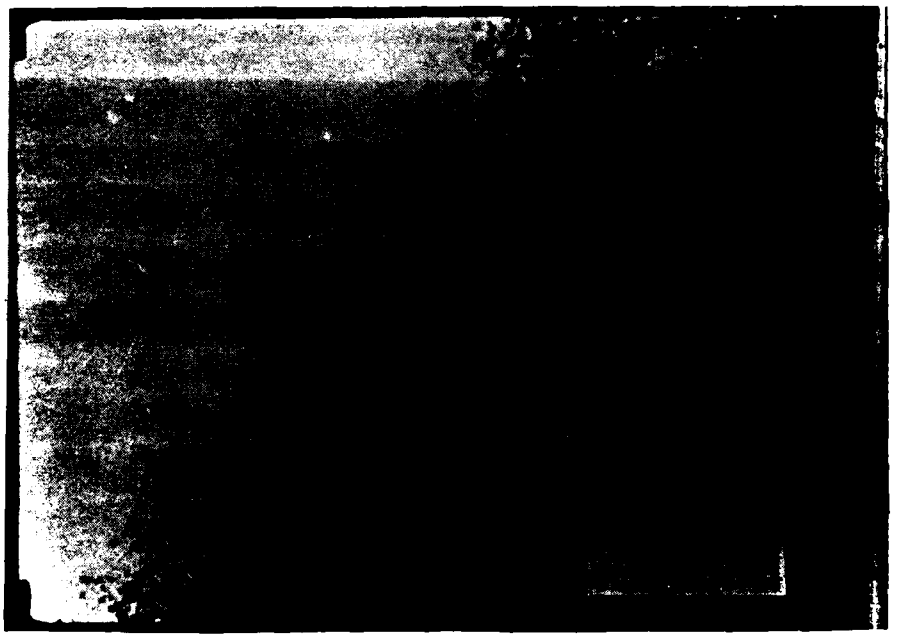

Figure 17 TEM photomicrograph from peritectic region of a 71 w/o chromium sample processed with purified inert gas.

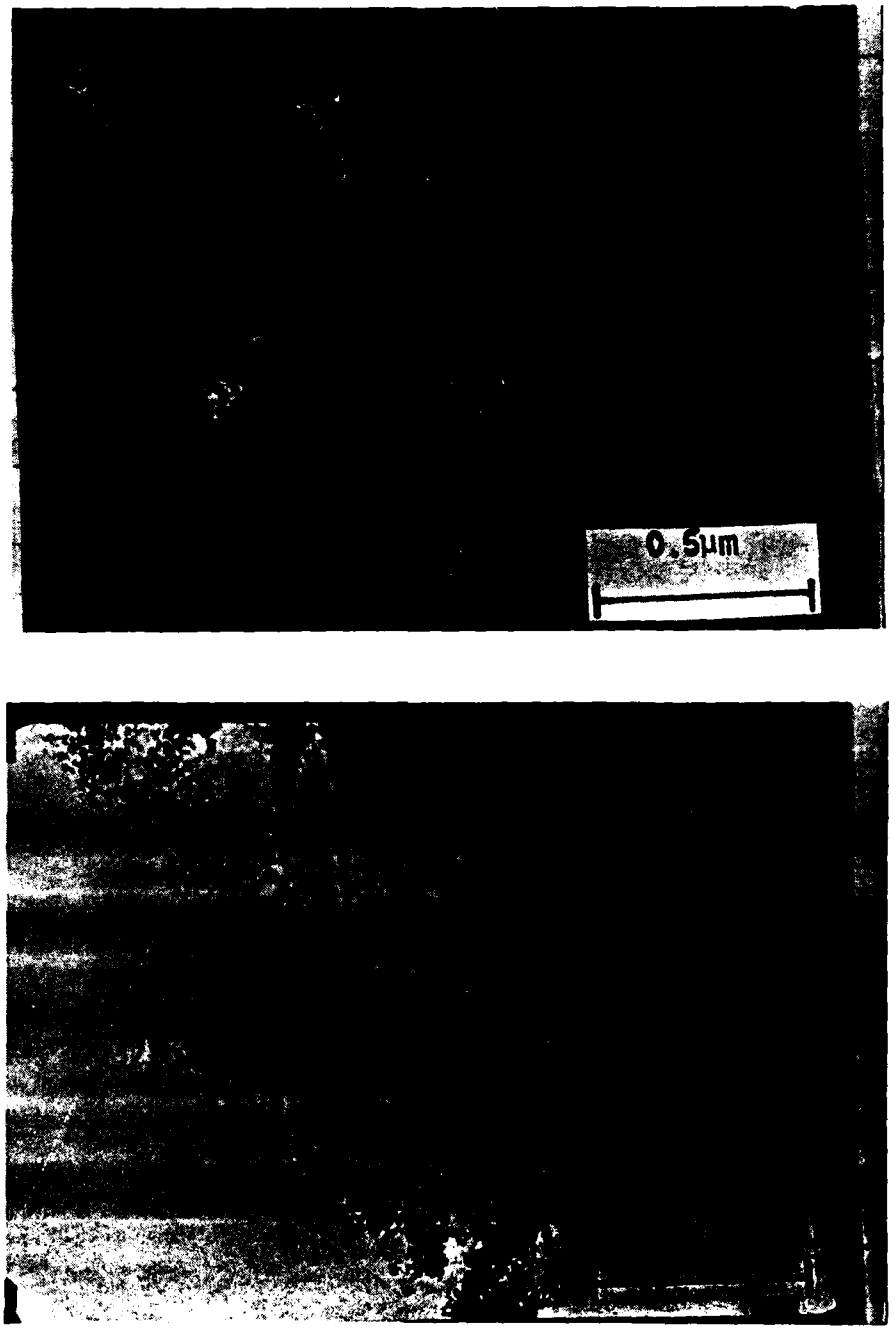

Figure 18 Comparison of darkfield and brightfield TEM photomicrographs form the interdendritic region of a 71 w/o chromium sample processed with purified inert gas.

Part B

Grain Refinement of Copper

by the Addition of Iron

and by Electromagnetic Stirring

INTRODUCTION

The importance of a fine equiaxed grains as opposed to columnar grains has long been recognized in a casting. Among various enhanced properties associated with a fine grain structure are improved low-temperature strength, reduced anisotropy, formability, and reduced segregation scale. The latter is especially important in castings that have to undergo homogenization; in a fine grain structure the characteristic diffusion distance and hence the homogenization time is reduced compared to a coarse grain structure. A number of techniques have been developed to produce fine grain structures during solidification[1]. The most common method is to add small amounts of grain refining agents, inoculants, to the melt just prior to casting. The additions either go into solution or remain as solids that act as heterogeneous nucleation catalysts during solidification. Examples of grain refining agents employed commercially for various alloys have been given in a recent review article by Monaolfo[2].

It is commonly accepted that the effectiveness of a grain refining agent is either due to enhanced heterogeneous nucleation rate or due to a reduction in the growth rate of the existing grains, thus allowing for further nucleation. However, the actual mechanism of grain refinement and hence the criteria which determine the effectiveness of one addition versus another are not fully understood. In general, the requirements for a good nucleating agent are higher interfacial energy between the inoculant and the melt, compared to that between the nucleated solid and the melt, and a good epitaxial fit between low index planes of the inoculant and the solid[3]. In addition, the inoculant particles should

be stable at the melt temperature, and should not agglomerate or float. A lower degree of lattice mismatch between the nucleant and the solid has been suggested as a possible criterion to determine grain refining potency of an inoculant[4]. In the absence of accurate surface energy data, Youdelis[5] has suggested the use of the "nucleation entropy" as a criterion for grain refining effectiveness. Based on this criterion, the larger the nucleation entropy, the more effective is the grain refiner. The solute build-up ahead of the solid-liquid interface, proposed by Tarsnis et al.[6], is another criterion for evaluating effectiveness of alloy additions. According to this criterion, the greater the solute build-up ahead of the interface, the more effective is the alloy addition in promoting grain refinement. Grain refining via peritectic reactions is another well known technique that is commercially employed in various alloys, especially in aluminum based alloys[7,8].

The grain refining techniques discussed above involve the deliberate addition of alloying elements or compounds to the melt. Equally important factors in determining the microstructure are the fluid flow and thermal conditions during solidification. The fluid flow can cause dendrite fragmentation by bringing hotter liquid to the root of the dendrite arms. The fragments, when carried away, can serve as growth sites for new grains. Improved fluid flow can come from a number of sources such as ultrasonic vibrations[9], mechanical stirring[10,11] or electromagnetic stirring[12]. The latter is being used extensively in casting industries, particularly for alloy compositions that have a strong tendency for centerline segregation and shrinkage porosity.

The present experiments were conducted to establish the role of the peritectic reaction and electromagnetic stirring in the grain refinement of copper-iron alloys. The effect of cooling rate and alloy compositions were also studied.

EXPERIMENTAL PROCEDURE

The experimental apparatus consisted of an electromagnetic levitation chamber, an inert gas purifying system, and a temperature monitoring device. Details of the apparatus can be found in an earlier paper[13]. The temperature of the levitated sample was measured and continuously monitored by a two-color pyrometer connected to a strip chart recorder. The pyrometer was calibrated against the melting points of pure iron, nickel, and copper to an accuracy of ±5°C. High purity helium, argon, and/or helium -2.0% hydrogen were continuously passed through the glass tube surrounding the sample to provide cooling and to protect the sample from oxidation. The oxygen content of the purified gas, continuously monitored using a solid state electrolyte, was in the range of 10^{-15}ppm.

The samples, each weighing about one gram, were prepared from 99.999% copper and 99.98% iron. The constituents for each sample, weighed to an accuracy of ±0.0001g, were arc melted in a titanium "gettered" helium atmosphere. The arc melted sample was lowered into the levitation coil, and the power to the coil was adjusted to levitate, melt and superheat the sample by approximately 300°C. The gas flow was then increased to solidify the sample at a rate of about 10-20°C/sec. The thermal arrest points corresponding to liquidus and peritectic

temperatures were recorded during repeated heating and cooling cycles of the levitated sample.

After determining the thermal arrest points, two different processing procedures were used to solidify the sample. One involved cooling the sample in the levitated state to 1000°C, at a rate of 10-20°C/sec, then quenching the solid sample in water from this temperature. The other involved quenching the sample from a temperature slightly above its liquidus temperature in water. The cooling rate of the water quenched samples is estimated to be approximately 500°C/sec[14]. The samples were sectioned, mounted, polished, and their average grain sizes were determined using a standard intercept technique[15].

RESULTS

The compositions, thermal arrest points, and the average grain sizes of the as quenched samples are summarized in Table I. The liquidus points and the peritectic temperature, as shown in figure 1, were found to be in good agreement, within the experimental errors, with the commonly accepted phase diagram[15]. Because of the oscillation of the sample in the levitated state, the temperatures could be measured with accuracy of ±10°C. The minimum concentration of iron required to have an iron rich primary phase, as detected by metallography and SEM, was found to be 2.8 wt.%. Following an earlier convention [Ref.16], alloys containing iron less than this value are termed "hypoperitectic", whereas those containing more iron are called "hyperperitectic".

The average grain size of samples quenched from their corresponding

liquidus temperatures as a function of the iron content is shown in figure 2. The error bars in this figure show the statistical variation of the mean. The average grain size of the pure copper when quenched from its melting point, not shown on this graph, corresponded to roughly 3mm. The results indicate that the addition of iron causes considerable grain refinement in copper, and the refinement increases with the iron content, as shown in figure 3 for two samples containing 0.57 and 2.05%Fe.

The effectiveness of iron as a grain refiner was further evidenced by the amount of bulk supercooling of the levitated melt. Although it was possible to supercool pure copper in excess of 400°C*, the addition of iron reduced this supercooling drastically. For example, when the alloy contained about 1% iron, the maximum supercooling was reduced to 100°C. At iron concentrations near the peritectic liquid and beyond, no appreciable supercooling was observed. A similar trend in the reduction of supercooling by the addition of iron was also noted by Southin & Weston[17].

In the composition range immediately surrounding 2.8 wt.% iron, from approximately 2.75 to 2.9 wt.%, the grain size showed considerable scatter. The variations in grain size can be seen in figure 4 for two samples containing 2.80 and 2.84%Fe. Over this rather narrow composition range, the scatter of the mean grain size of individual samples fell outside the confidence intervals of each sample. The scatter appears to be due to the possible alternative nucleation

* In several occasions, pure copper samples were supercooled considerably below the lower limit of pyrometer detection which was 700°C.

sequences, caused by supercooling, and suppression of the primary phase formation or the peritectic reaction.

When the concentration of iron exceeded 2.9 wt.%, the grain size showed a continued decrease with increasing iron concentration. The microstructures encountered in this region are shown in figure 5, where the primary gamma iron appears as dark particles scattered uniformly throughout the sample. The data points in this region, however, do not seem to follow the continuation of the curve for the hypoperitectic region. This trend will become more obvious when the results of the samples solidified while levitated state are considered later. In addition, the grain size of the hyperperitectic samples had greater uniformity as compared to the hypoperitectic samples.

The effect of iron content on the mean grain size of the alloys solidified in the levitated state is shown in Figure 6. For the hypoperitectic alloys, the grain size showed the same trend as the water quenched samples. It should be noted that the cooling rate during solidification of the levitated samples was around 20°C/sec, as compared with about 500°C/sec for the water quenched samples.

In alloys containing greater than 2.8% Fe, the grain size of the samples solidified in the levitated state was found to be insensitive to the iron concentration, as indicated in figure 6. This can also be seen from the photomicrographs shown in figure 7 for two samples containing 3.27 percent and 7.46 wt.% iron--In spite of the large difference in iron concentrations, the average grain size is the same in both samples. At lower iron concentrations, the iron dendrites are small with only a few side branches. At larger concentrations, however, the

dendrites have a well developed dendritic structure consisting of numerous secondary, and in some cases, tertiary arms. It was also noted that primary dendrites had accumulated mostly near the surface of the samples. Solid state precipitates of iron, approximately 0.4 microns in diameter, were also seen in the copper matrix by SEM analysis. This is in contrast with the water quenched samples which showed no iron precipitates, indicating that the copper matrix was a supersaturated alpha solid solution.

Discussion

The results of the present investigation indicate that the addition of iron causes considerable grain refinement in copper, in agreement qualitatively with earlier studies[18,19,20]. In the earlier studies the effect of iron was studied on either multi-component commercial alloys or elements such as phosphorus were used to deoxidize the melt. In the present research, high purity materials were used, and the samples were levitation melted in an essentially oxygen free atmosphere. The inherent advantages of this technique include noncontamination, melt homogeneity, and precise temperature, time and atmospheric control. Because of these features, the present results most likely show the grain refining effects due to the iron additions only.

In the hypoperitectic region, the grain size in both sets of samples, quenched in water or solidified in the levitate state, decreased as the iron concentration was increased. In the hyperperitectic region, however, the grain size of the alloys solidified in the levitate state showed no dependence on the iron content, whereas

those quenched from their liquidus showed a continued decrease as the iron content was increased. The two sets of data are compared in figure 8.

In the hypoperitectic region, the grain refinement mechanism by the addition of iron can be discussed based on the amount of solute build up ahead of the interface criterion, denoted as the "P" factor[6], or the nucleation entropy criterion[5]. The calculated values of the nucleation entropy and the P factor at 1wt% Fe are -4.322 J· mole $^{-1}$·K^{-1} and 1.30, respectively. The thermodynamic values necessary for the calculations were obtained from the JANAF tables[21] and the phase diagram. Since these quantities increase with increasing the iron content, both criteria qualitatively explain the enhanced grain refinement with increased iron content. However, neither criteria can be used a priori to predict grain refinement capability of iron. This is due to the fact that the minimum value of the p factor or the nucleation entropy necessary for effective grain refinement is not yet well established. For aluminum binary alloys, it was shown that a p factor larger than about 20 was necessary to cause 80% reduction in the grain size[6]. At lower values, the grain size reduction was considerably lower. For the Cu-Fe system, even though the p factor is small, less than 2, the grain size reduction is larger than 90%.

As indicated earlier, the effectiveness of iron additions on the nucleation of the copper in the hyperperitectic region can be judged based on the amount of bulk supercooling attainable in the samples. Similar to other experiments[17], it was observed that the bulk supercooling reduced drastically as iron concentration was increased. Youdelis[5] has attributed the reduction in the supercooling to the

increased nucleation entropy with solute concentration.

In the hyperperitectic region, the grain refinement could possibly be due to either the growth restrictive nature of the peritectic reaction or the presence of iron primaries acting as heterogeneous nucleation sites. The disregistry between γ-iron and copper at the peritectic temperature is only 0.8%, indicating the potency of iron primaries in nucleating the copper phase. It was noted that no appreciable supercooling at the peritectic temperature was observed in the hyperperitectic alloys, which again indicates the effectiveness of iron in nucleating copper. This can be compared with the results of our experiments with Cu-Nb alloys where a supercooling of approximately 10°C was observed at the peritectic temperature[22]. For Cu-Nb system, the overall lattice mismatch between (111) planes of copper and (110) planes of niobium is around 14.5%.

To compare the results of the water quenched samples with those solidified in the levitated state two points must be taken into consideration: (1) the latter samples were solidified at a much lower cooling rate than the former ones (20°C/sec compared with 500 °C/sec, respectively), (2) and the latter samples were solidified while being stirred by the electromagnetic field. Despite the lower cooling rates, the average grain size of the latter samples in the hypoperitectic region was comparable to that of the water quenched samples. The results indicate the beneficial effect of fluid flow on grain refinement in this region. In the hyperperitectic region, however, the grain size of the samples solidified in the levitated state was considerably larger than that of the water quenched samples. In fact, the grain size became

insensitive to the iron content, indicating the detrimental effect of electromagnetic stirring. This is due to the fact that while stirring can cause dendrite fragmentation or remelting, it can also enhance coarsening and agglomeration of the nucleating particles. The first effect will result in grain refinement via grain multiplication, whereas the second will reduce the number of heterogeneous nucleation sites. The relative importance of the two would depend on the alloy composition, cooling rate, as well as the flow conditions.

It is believed that in the hypoperitectic region, the grain multiplication mechanism has augmented the effect of iron in promoting grain refinement such that the grain size of the slowly cooled samples were the same as the rapidly cooled ones. In the hyperperitectic region, on the other hand, the increased fluid flow has caused appreciable coarsening and agglomeration of the primary iron phase, diminishing their effectiveness to nucleate the copper. The stirring also caused preferential accumulation of the iron primaries on the surface of the samples. The agglomeration phenomenon is similar to the commonly observed fading process, as a result of which the effectiveness of the inoculants is found to diminish as the metal is held in the liquid state. For conventional casting processes, the fading process occurs over a period of minutes. In the case of electromagnetic levitation, the increased fluid flow enhances the process appreciably.

Conclusions.

The addition of iron in the range of 0.57 to 7.5 wt.% has been found to cause appreciable grain refinement in copper. In the hypoperitectic alloys, electromagnetic stirring enhances the grain refinement via the grain multiplication mechanism. In the hyperperitectic alloys, on the other hand, the stirring reduces the grain refining capability of iron by agglomerating the primary iron particles which act as heterogeneous nucleation sites for copper.

References

1. G. J. Abbaschian and S. A. David: Grain Refinement in Castings and Welds, Conf. Prod. St. Louis, Oct. 25-26, 1982, Pub. Met. Soc. AIME., 1983.

2. L. F. Mondolfo: in Reference 1, pp.3-50.

3. P. B. Crosley, A. W. Douglas and L. F. Mondolfo: Iron and Steel Inst. Pub. 119, 1967, pp.10-17.

4. D. Turnbull and B. Vonnegut: Ind. and Eng. Chem., 1952, vol. 44, pp. 1292-1298.

5. W. V. Voudelis: Metal Sci. Sept., 1979, pp. 540-543.

6. L. A. Tarshis, J. L. Walker, and J. W. Rutter: Metall Trans., 1971, vol. 2, pp. 2589-2597.

7. F. A. Crossley and L. F. Mondolfo: J. Metals. 1951, vol. 3, pp. 1143-1148.

8. L. Arnberg, L. Backerad, and H. Klang; in Reference 1, pp. 165-181.

9. A. H. Freeman and J. F. Wallace: J. Metals. 1957 Trans AFS 1957, vol. 65, p.578-589.

10. D. Spencer, R. Mehrabian, and M. C. Flemings: Metall. Trans., 1972, vol. 3, p. 1925-1932.

11. S. D. E. Ramati, G. J. Abbaschian, and R. Mchrabian: Metall. Trans. B, 1978, vol. 9B, pp.241-245.

12. M. Gray, A. McLean, G. Weatherly, R. J. Simcoe, R. Hadden and L. Beitelman: ISSM, April 1982, pp. 20-25.

13. G. Amaya, J. A. Patchett, and G. J. Abbaschian, In Reference 1, pp.51-65.

14. G. J. Abbaschian and M.C. Flemings: Metall. Trans. A., 1983, vol. 14A, pp. 1147-1157.

15. Metal Handbook, 1973, vol. 8 ASM, p. 293.

16. R. M. Kotschi and C. R. Loper Jr.: AFS Trans., 1977, vol. 85, pp.425-430.

17. R. J. Southin and G. M. Weston, J. Aust. Inst Metals 1973, vol. 18, p.74-81.

18. K. Iwase, J. Asato and N. Nasu: Science Report Tohoku Imp. Univ., Honda Anniv.vol. 1936, pp.652-669.

19. A. Cibula: J. Inst. Metals, 1953-54, vol. 82, pp.513-524.

20. G. C. Gould, G. W. Form and J. F. Wallace: Modern Castings, 1960, Vol. 37, No. 5, pp. 144-152.

21. JANAF: Thermochemical Tables, 2nd ed., National Standard Reference Edition, 1971.

22. G. J. Abbaschian: ONR Technical Report 2, Office of Naval Research, Contract N090014-81-K-0730, NR031-836, Oct. 1983.

23. El-Kaddah and J. Szekely: Metall. Trans. B, 1983, vol. 14B, pp. 401-410.

TABLE I

Thermal Arrest Points and Grain Size Measurements for Copper-Iron Alloys

Quenched in water

Wt%Fe	Peritectic °C	Liquidus °C	Quenching Temp.°C	Grain Size,mm
0.57	1080	--	1085	0.330 ± .170
2.05	1080	--	1090	0.130 ± .050
2.80	1094	1094	1100	0.070 ± .020
2.84	1100	1100	1115	0.035 ± .008
3.08	1124	1100	1140	0.032 ± .010
3.12	1150	1094	1160	0.021 ± .004
3.20	1140	1090	1150	0.032 ± .007
3.42	1170	1100	1185	0.037 ± .007
3.67	1150	1094	1260	0.030 ± .008
4.06	1190	1090	1265	0.022 ± .008
		Solidified in the Levitated State		
0.72	1090	--	1000	0.210 ± .090
1.65	1080	--	1000	0.200 ± .040
2.14	1090	--	1000	0.110 ± .040
2.67	1080	--	1000	0.120 ± .040
2.72	1094	--	1050	0.052 ± .008
2.80	1100	--	1000	0.220 ± .080
2.81	1094	--	1000	0.110 ± .040
2.86	1110	1094	1000	0.042 ± .010
3.27	1170	1100	900	0.073 ± .026
3.35	1160	1090	1000	0.071 ± .020
7.46	1280	1094	1000	0.072 ± .015

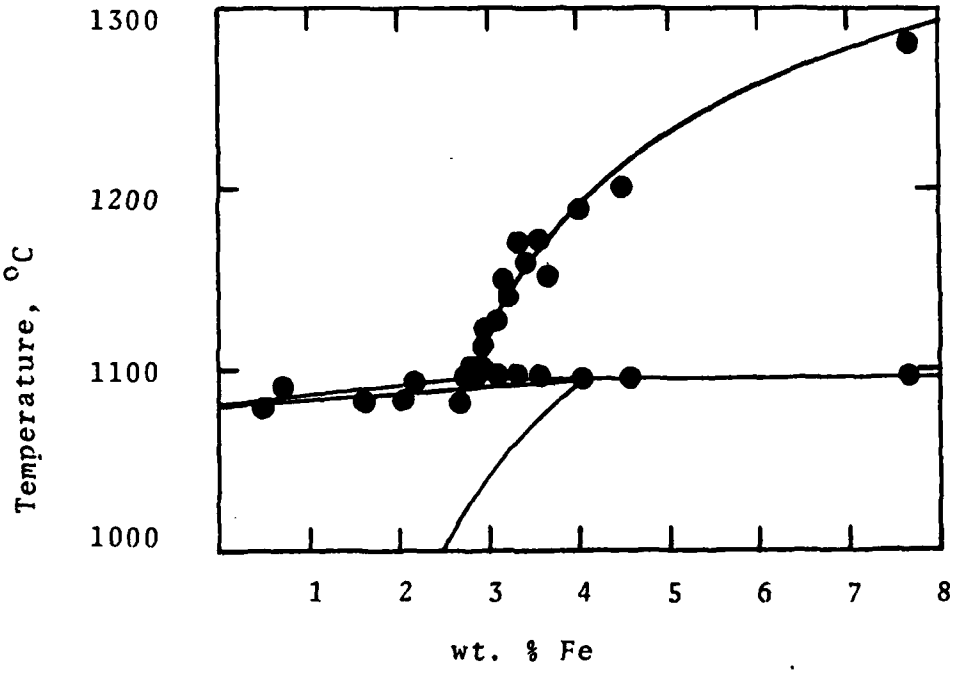

Figure 1: The copper-iron phase diagram on the copper rich side, with the measured liquidus and peritectic temperatures.

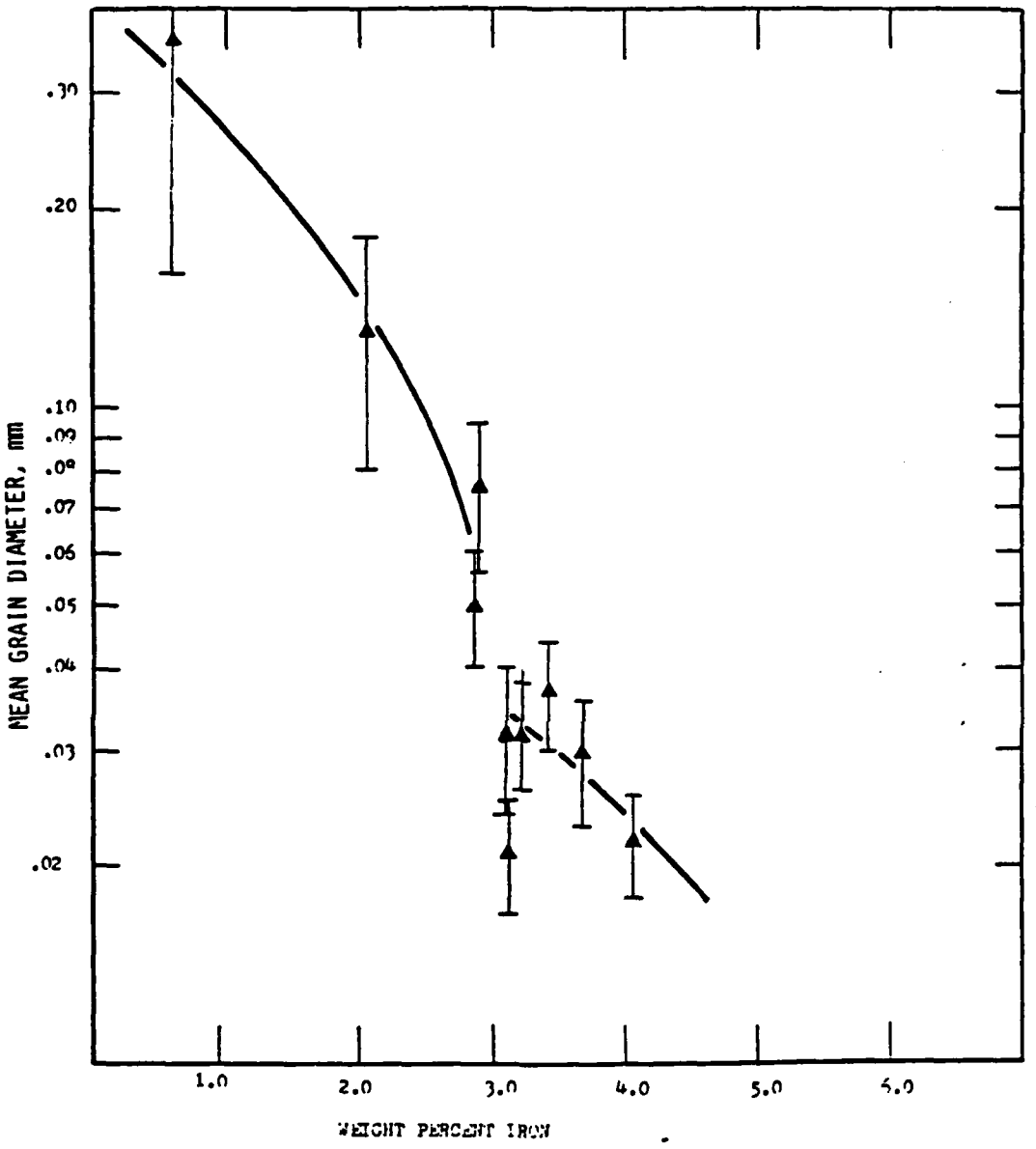

Figure 2: Mean grain size vs iron content for samples quenched in water from their liquidus.

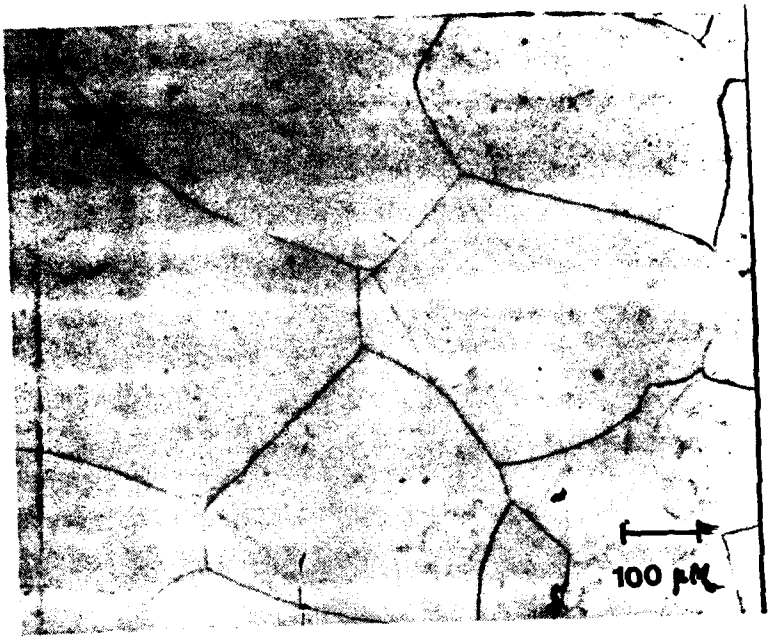

a

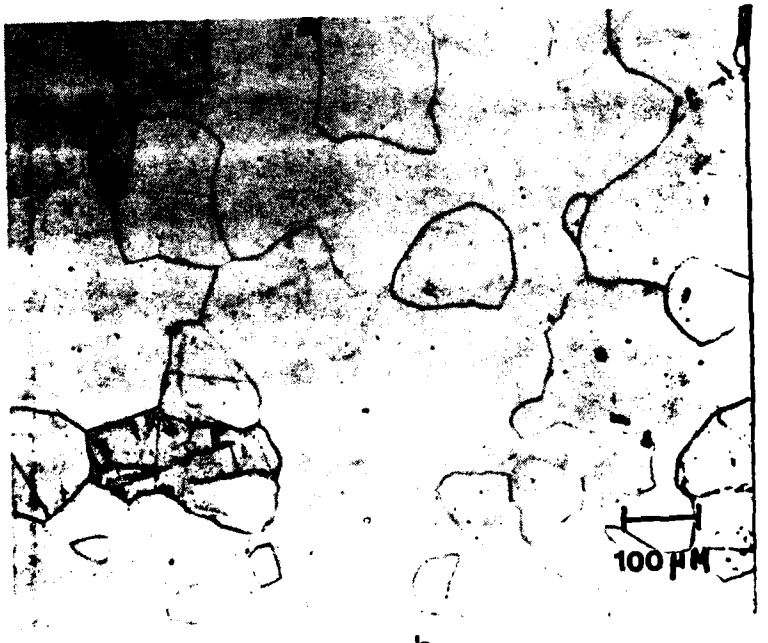

b

Figure 3: Grain size of water quenched hypoperitectic alloys a) 0.57 and b) 2.05%Fe

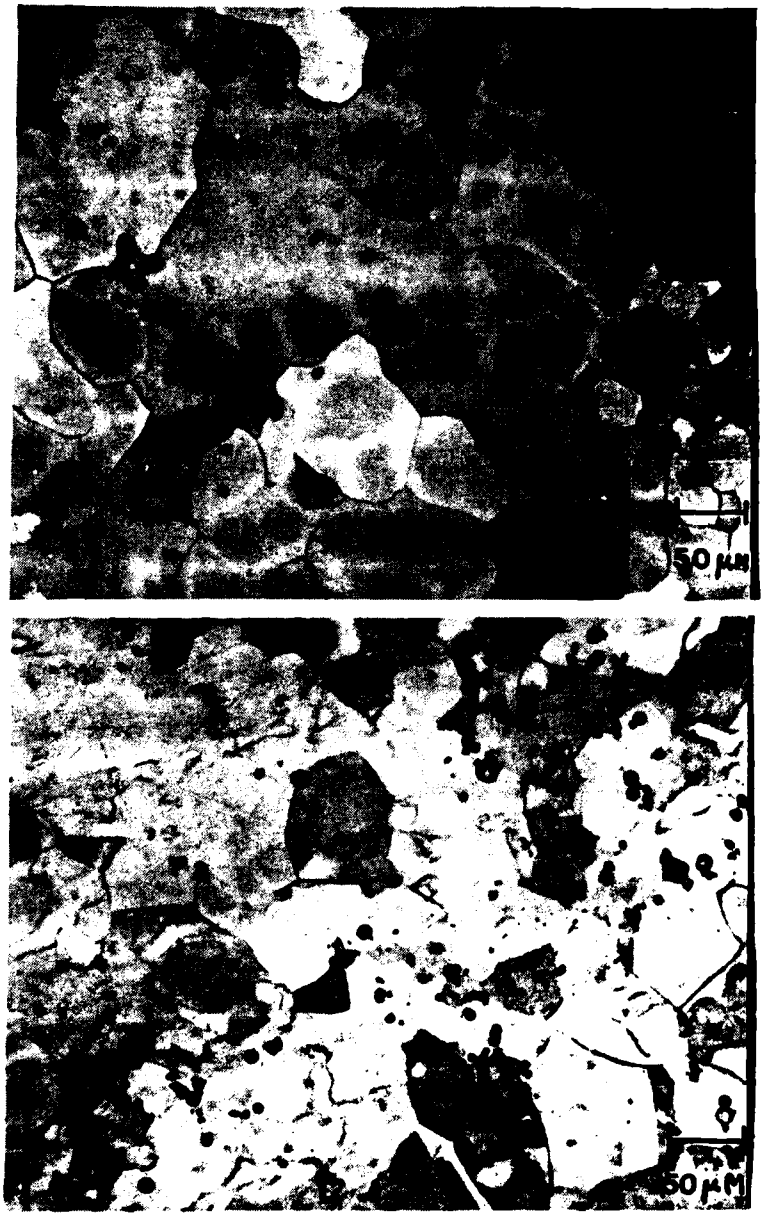

Figure 4: Microstructures of two samples with 2.8% Fe solidified in levitated state - note the difference in the grain size.

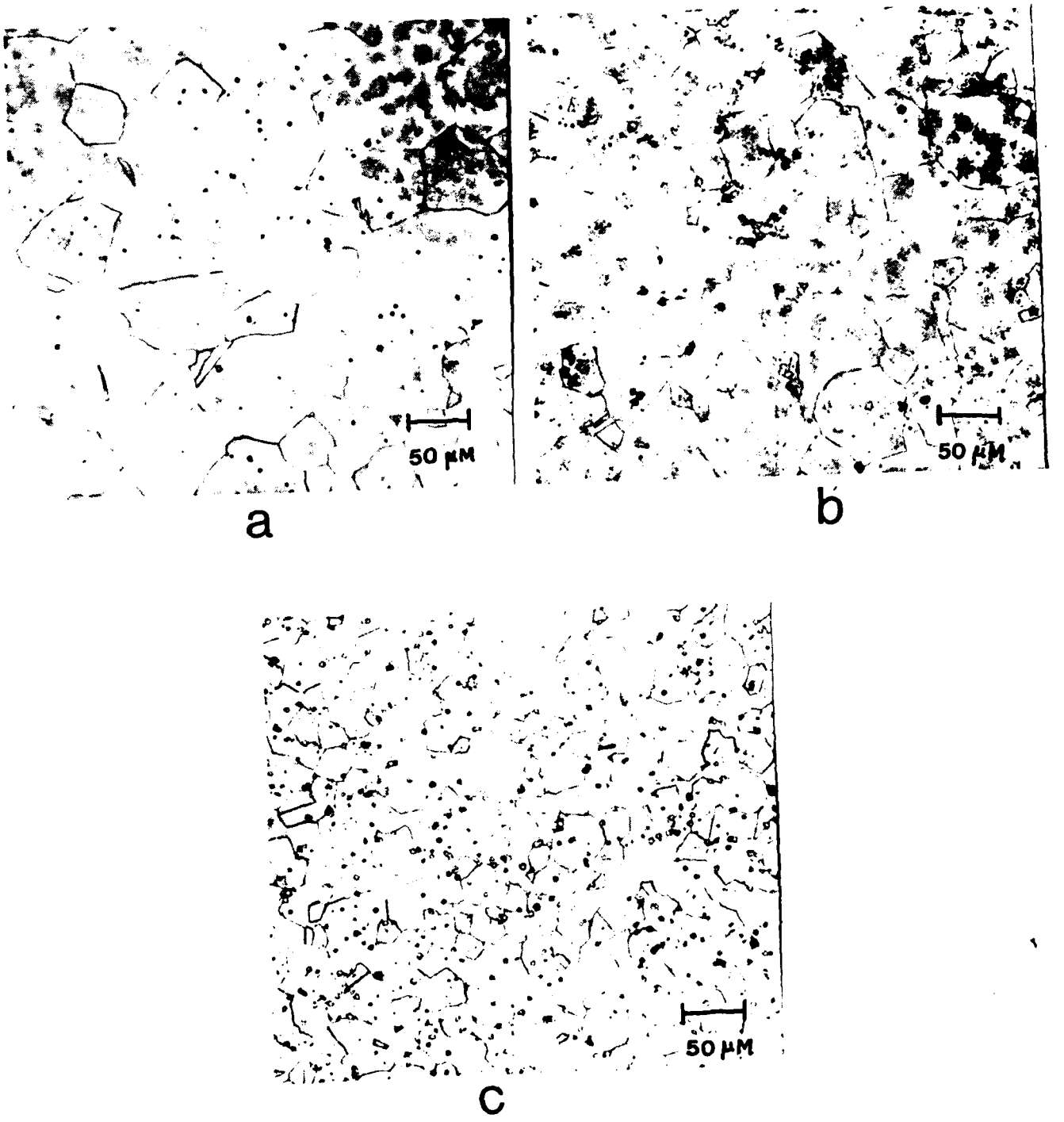

Figure 5: Effect of iron additions on the grain size of copper in water quenched hyperperitectic alloys (a) 2.84 (b) 3.12 and (c) 4.06wt%Fe.

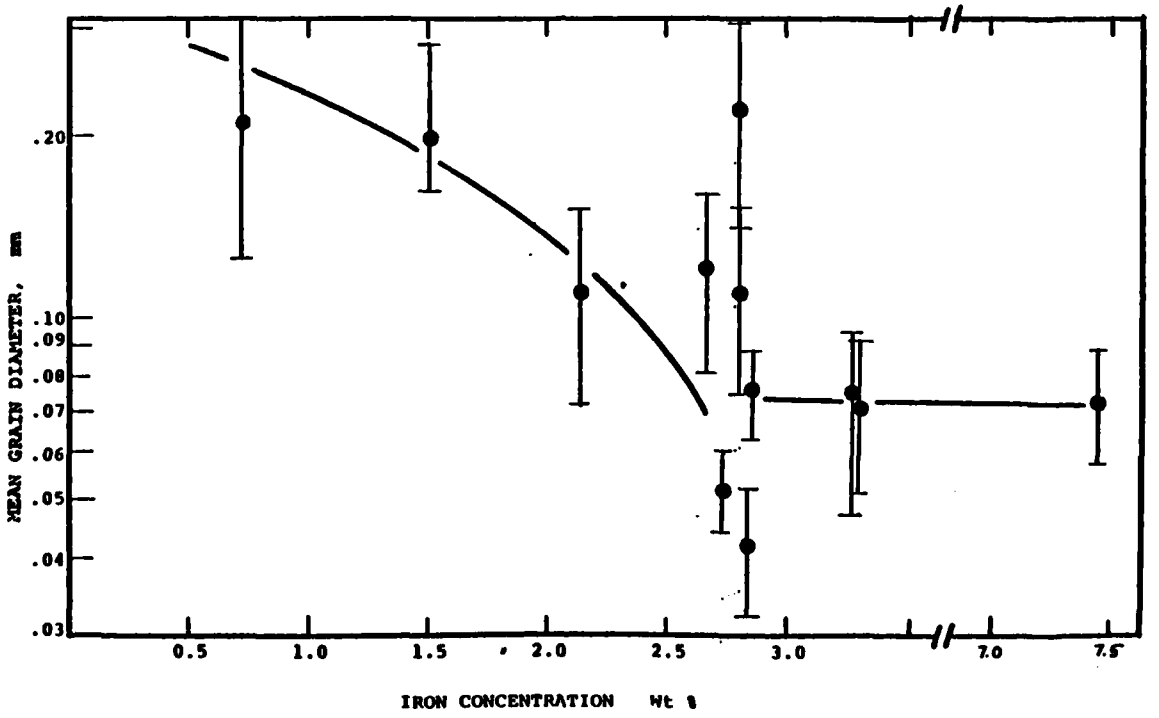

Figure 6: Mean grain size as a function of iron content for copper-iron alloys quenched in water from 1000°C.

a

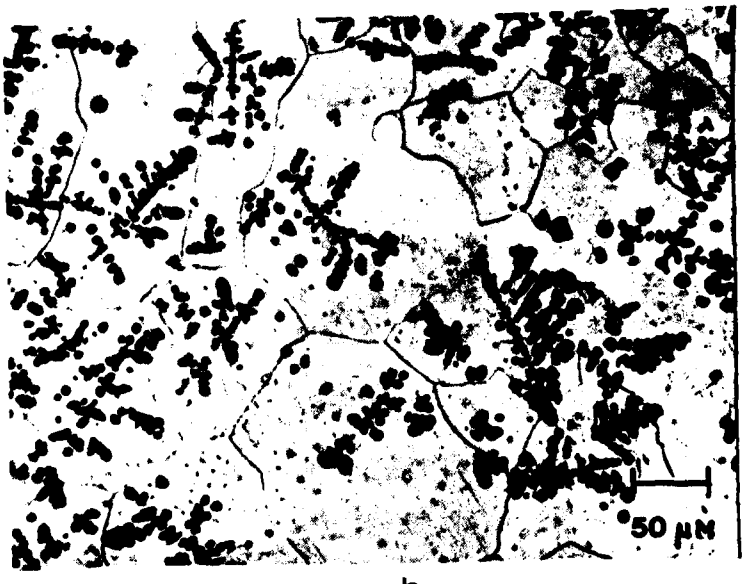

b

Figure 7: The effect of iron addition on the grain size of hyperperitectic alloys solidified in the levitated state a) 3.27 and b) 7.46%Fe.

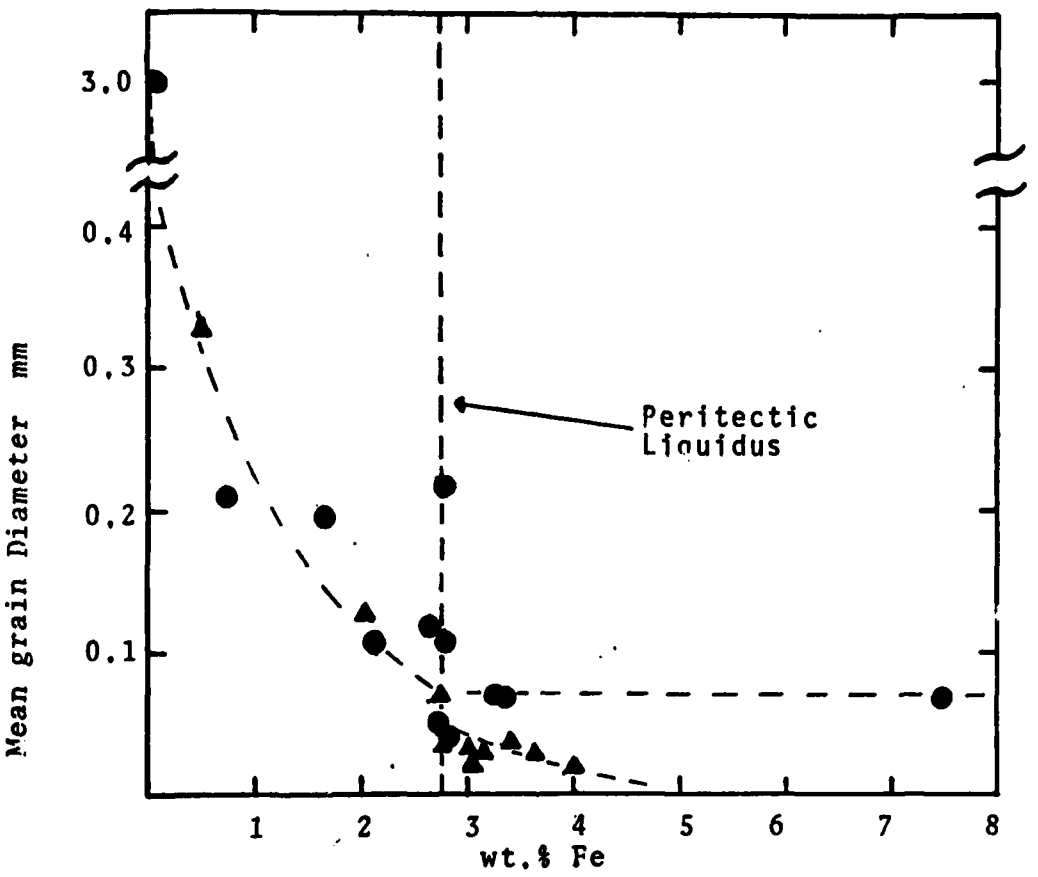

Figure 8: The effects of cooling rate,stirring, and iron concentration on the mean grain size of copper iron alloys.

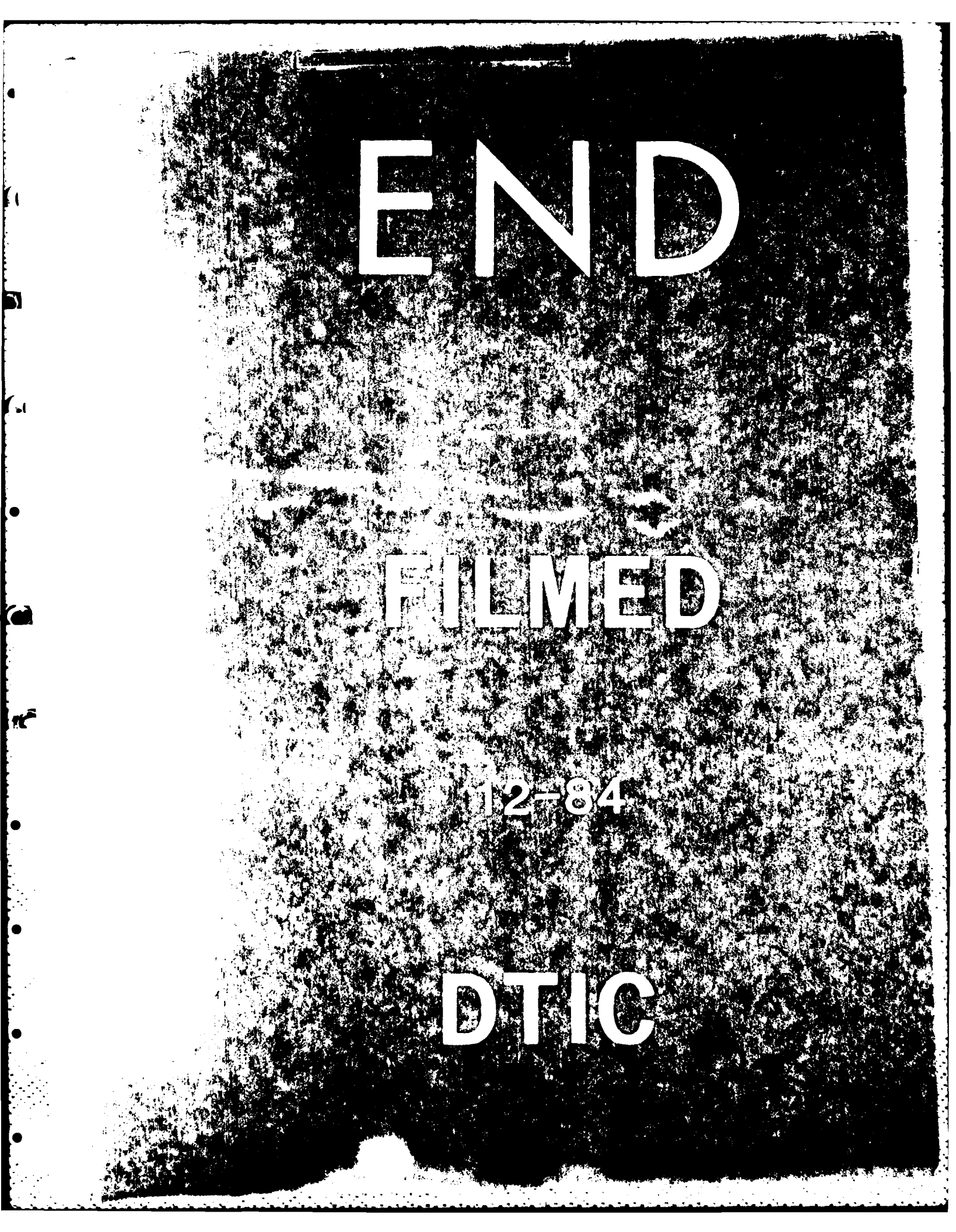
END
FILMED
12-84
DTIC